DIPLOMARBEIT

Analysis and modeling of melting processes in phase change materials for use in latent heat storages

zur Erlangung des akademischen Grades

Diplom-Ingenieur/in

im Rahmen des Studiums

Technische Physik

eingereicht von

Robert Pejic, BSc.
Matrikelnummer 01225739

ausgeführt am Institut für Festkörperphysik
der Fakultät Physik der Technischen Universität Wien
(in Zusammenarbeit mit dem AIT)

Betreuung
Betreuer/in: Associate Prof. Dipl.-Chem. Dr.rer.nat. Andrey Prokofiev
Mitwirkung: Dr. Klemens Marx

Wien, 08.10.2018 _____ _____

(Unterschrift Verfasser/in) (Unterschrift Betreuer/in)

Acknowledgements

Firstly, I would like to thank Klemens Marx, Tilman Barz, Wolfgang Hohenauer and the Austrian Institute of Technology for giving me the chance to work on a very interesting subject matter and providing to me the research residence.

Furthermore, I want to express my sincere gratitude to my professor Andrey Prokofiev, who took on the role as supervisor from the side of the Technical University of Vienna. He provided me with great guidance and professional academic feedback. I am deeply grateful for his expertise and assistance during the conduction of this thesis.

Last but not the least, I would like to thank my family and my fiance for supporting me not only morally but also with proofreading my thesis.

Abstract

This master thesis investigates the delay of the melting process (difference between the temperatures T_{Start} and T_{On}) for phase change materials (PCM) that is observed in differential scanning calorimetry (DSD). The goal of this thesis is to analyse the delay in more detail and reveal the effect of thermal conduction on the shift of the melting point. Knowledge about the temperature range of phase transitions is of great importance for the performance of latent heat thermal energy storages (LHTES).

To shed more light onto this matter, the DSC process is analysed in detail to develop a model for numerical simulations. In the end the DSC process is reduced to a one dimensional heat conduction problem.

In the beginning of this thesis, the basics of thermodynamics and the differential scanning calorimetry process is discussed, followed by an introduction to the aforementioned model and explaining the used numerical method. Afterwards, the model is tested and verified with a well-known standard, namely sapphire. Finally, the simulation was carried out for the PCM, which resulted in the finding, that thermal conduction was accountable for the delay extent decreasing with the heating rate. The existence of the delay itself is due to a different reason, which will be discussed in the theoretical section of the thesis.

Kurzfassung

Diese Masterarbeit untersucht die Verzögerungen des Schmelz- und Erstarrvorganges (Differenz zwischen den Temperaturen T_{Start} und T_{On}) für Phasenwechselmaterialien (PCM) welche in der Differentialkalorimetrie (DSC) beobachtet wird. Das Ziel dieser Arbeit ist es die Verzögerung aufzuzeigen und den Effekt der Wärmeleitung auf die Verschiebung des Schmelzpunktes zu untersuchen. Wissen über die Breite des Phasenwechsels ist von großer Bedeutung für die Leistung von latent heat thermal energy storages (LHTES).

Um mehr Licht auf das Problem zu werfen wird der Prozess der DSC detailiert analysiert um ein Model für numerische Simulationen zu entwickeln. Letztendlich wird der DSC Prozess auf ein eindimensionales Wärmeleitungsproblem reduziert.

Am Anfang der Arbeit werden die Grundlagen der Thermodynamik und DSC diskutiert, gefolgt von der Einführung des Models mit den verwendeten numerischen Methoden. Anschließend wurde das Model getestet und mit dem bekannten Standard Saphir bestätigt. Schlussendlich wurde die Simulation für das PCM ausgeführt, worauf man den Schluss ziehen kann, dass die Wärmeleitung verantwortlich für die verschieden große Ausprägungen der Verzögerung ist. Die Existenz der Verzögerung ist auf einen anderen Grund zurückzuführen, welcher auch in dem theroetischen Abschnitt der Arbeit erörtert wird.

Contents

Introduction

The energy industry often has to deal with the problem of intermittent and unpredictable energy income. For example, solar energy is a completely irregular energy source which is in addition also only available during day time. Similar problems rise in heat recovery systems, where the waste heat availability and utilization periods are different. For the purpose of storing energy for later use, *thermal energy systems (TES)* are being used. [5]

Apart from sensible heat storages, especially *latent heat thermal energy storages (LHTES)* are attractive for domestic applications (phase change temperature in the low temperature range between 0° and 200° C). LHTES use *phase change materials (PCM)* to store energy. They are particularly interesting, because they have higher thermal energy storage density while requiring smaller masses and volumes of material. A problem that arises in LHTES is that, the temperature range during the phase change is affected by storage loading operating condition, i.e., heating and cooling rates of the PCM. Since PCMs with a narrow temperature range during the phase transition (melting/solidification) have better performance [13], it is necessary to analyse the behavior of phase change materials during the transition for multiple heating rates. This thesis will analyse specifically a high density polyethylene (HD-PE). When this PCM is subjected to a *differential scanning calorimetry (DSC)*, for different heating and cooling

rates a delay (difference between the temperatures T_{Start} and T_{On}) of the melting and solidification process can be observed. With this, the shift of the melting temperature to higher values for lower heating/cooling rates is meant. In this thesis the cause for the delay is discussed and the effect of the thermal conduction is investigated.

The goal of this thesis is to quantify the process of the DSC by analysing the experimental setup as well as the sample itself. A model is developed, that simplifies the complexities of the thermal processes inside the DSC crucible. Given the nature of the problem, it is possible to break it down into a simple problem which neglects convection as well as radiation. With this, the DSC process can be reduced to a one dimensional heat conduction problem. This then renders it possible to determine the role of heat conduction in this phenomenon.

The simulation itself has been tested beforehand with sapphire ($\alpha - Al_2O_3$), a substance with well known properties. Sapphire, a standard defined by the *National Bureau of Standards (NBS)*, is normally used for DSC measurements *(see App. A)*. After the successful affirmation of the developed simulation technique, the DSC process then was modelled.

The device used for collection of the experimental data set is a heat flux DSC 204 F1 Phoenix.

Fundamentals

2.1 Heat transfer

The basics of heat transfer that are discussed in this chapter are elucidated in more detail in the following literature [3, 10, 12].

The concept of heat as a process function is established in the first law of thermodynamics

$$\Delta U = \Delta Q + \Delta W \tag{2.1}$$

It basically predicates, that energy that is added to an system in form of heat ΔQ, can for one thing increase the internal energy U of the system which correlates with the temperature, for another thing lead to an expansion of the matters volume (the system then has to perform the work ΔW). In principle the first law of thermodynamics is a law of energy conservation.

Heat transfer only occurs if spatial temperature differences are present. According to the second law of thermodynamics the heat then is transported in the direction of a lower temperature. For further discussion several parameters are introduced.

The heat flux, or heat flow rate $\dot{Q}$ describes the heat that is transferred per unit of time ($[\dot{Q}] = \mathrm{J\,s^{-1}} = \mathrm{W}$)

$$\dot{Q} = \frac{dQ}{dt} \tag{2.2}$$

and the heat flux density $\dot{q}$ denotes the heat flux per unit area ($[\dot{q}] = \mathrm{W/m^2}$)

$$\dot{q} = \frac{d\dot{Q}}{dA}. \tag{2.3}$$

In general three different mechanisms of heat transfer exist, heat conduction, convection and radiation.

2.1.1 Heat Conduction

Heat is transferred by principle energy carriers: atomic core vibrations in form of phonons (quasi-particles that describe quantized vibrational waves in the lattice), electrons and fluid particles. These pass on the kinetic energy to the adjacent atoms/molecules, which results in a heat transfer. For this effect no macroscopic movement is necessary, it is a purely microscopic phenomenon.

Fourier's law lays the foundation of heat conduction [10]

$$\dot{q}_x = -\lambda \frac{dT}{dx} \tag{2.4}$$

whereas λ is the thermal conductivity ($[\lambda] = \mathrm{W\,m^{-1}\,K^{-1}}$). If a local temperature gradient is present, then the heat flux density is proportional to it and depends on the thermal conductivity. For an isotropic material the following relation is obtained

$$\vec{q} = -\lambda \nabla T. \tag{2.5}$$

Heat equation

The heat equation can be obtained by formulating an energy balance

$$\Delta E_{total} = E_{in} - E_{out} \tag{2.6}$$

where ΔE_{total} is the change of the system's entire energy. The change is induced by the energies that enter (E_{in}) and exit (E_{out}) the system in form of heat. With this approach one obtains the heat equation (see App. B)

$$\rho c_p \frac{\partial T}{\partial t} = \frac{\partial}{\partial x}\left(\lambda \frac{\partial T}{\partial x}\right) + \frac{\partial}{\partial y}\left(\lambda \frac{\partial T}{\partial y}\right) + \frac{\partial}{\partial z}\left(\lambda \frac{\partial T}{\partial z}\right) \tag{2.7}$$

With the simplification of spatially uniform physical characteristics the equation changes to

$$\frac{\partial T}{\partial t} = a \nabla^2 T \tag{2.8}$$

whereby $a = \dfrac{\lambda}{c_p \cdot \rho}$ is the thermal diffusivity ($[a] = \mathrm{m}^2/\mathrm{s}$).
In cylindrical coordinates the heat equation takes the following form (see App. C)

$$\rho c_p \frac{\partial T}{\partial t} = \frac{1}{r}\frac{\partial}{\partial r}\left(\lambda r \frac{\partial T}{\partial r}\right) + \frac{1}{r^2}\frac{\partial}{\partial \varphi}\left(\lambda \frac{\partial T}{\partial \varphi}\right) + \frac{\partial}{\partial z}\left(\lambda \frac{\partial T}{\partial z}\right). \tag{2.9}$$

For a cylinder, where the heat conduction happens only in axial direction, the r and ϕ-coordinates simply disappear and the equation is then simplified as follows

$$\rho c_p \frac{\partial T}{\partial t} = \frac{\partial}{\partial z}\left(\lambda \frac{\partial T}{\partial z}\right). \tag{2.10}$$

With the relations between the enthalpy and the specific heat capacity for an isobaric process

$$dh = c_p \cdot dT \tag{2.11}$$

the equation can be written in the following enthalpic form [4]

$$\frac{\partial(\rho h)}{\partial t} = \nabla \cdot (\lambda \vec{\nabla} T) \tag{2.12}$$

whereby $h = \frac{H}{m}$ is the specific enthalpy ($[h] = \frac{J}{kg}$).

2.1.2 Convection

Convection is a phenomenon of the heat transfer through movement of macroscopic parts of fluids or gases with different temperatures drives by buoyancy. The heat transfer between different states of matter (e.g. solid and fluid) depends on the temperature difference as well as on various other factors, such as temperature profile, velocity profile, geometry and physical characteristics which are taken all together into the parameter α ($[\alpha] = \mathrm{W/m^2/K}$)

$$\dot{q} = \alpha(T_{Phase1} - T_{Phase2}). \tag{2.13}$$

whereas T_{Phase1} and T_{Phase1} depict the temperatures of two dissimilar phases. The transition coefficient α can be characterized with the similitude theory. However, this theory will not be discussed in this thesis. For more details on convection refer to the following literature [10, 12].

2.1.3 Radiation - thermal exchange

Thermal radiation is the third mechanism of heat transfer. This is thermal exchange via electromagnetic waves emitted and absorbed by matter. The radiation does not require the presence of a medium. Since radiation from the interior molecules is strongly absorbed by the adjoining particles, their emission contribution is negligible and therefore the radiation from a solid or liquid is a surface phenomenon. The power that is released per unit area of the surface is given by the Stefan-Boltzmann law

$$P = \varepsilon\sigma \cdot T^4 \tag{2.14}$$

where σ is the Stefan-Boltzmann constant and ε is the emissivity. Due to the low temperatures of the differential scanning calorimetry measurements the radiation effect is negligible and thus radiation will not be discussed in detail. For more details on radiation refer to the following literature [10, 12].

2.2 First order phase transitions

The thermodynamic state of a physical system can be described with the following thermodynamic potentials.

- Internal energy U
- Free energy F
- Enthalpy H
- Gibbs free energy G

These are functions of the thermodynamic state variables temperature T, pressure p, volume V and entropy S.

Variation of these parameters changes the thermodynamic state of a phase, but at some values of the parameters the matter experiences a transition into another thermodynamic phase. The phase transition of interest for this thesis is the change of the material from solid to fluid - the melting. This kind of phase transition belongs to phase transitions of first order.

What order a transition has is defined by the Ehrenfest's classification scheme. It says, that the order of a transition is the order of the lowest differential of the Free Energy G which shows a discontinuity. For a I order phase transition the first derivatives of G - the entropy and the volume - have discontinuities

$$\left(\frac{\partial G}{\partial T}\right)_p = -S, \qquad \left(\frac{\partial G}{\partial p}\right)_T = V \tag{2.15}$$

The II order phase transitions have discontinuities in the second derivatives of G. This time the response functions

$$\left(\frac{\partial^2 G}{\partial T^2}\right)_p = -\frac{c_p}{T}, \qquad \left(\frac{\partial^2 G}{\partial p^2}\right)_T = -V\kappa_T, \qquad \left(\frac{\partial^2 G}{\partial T \partial p}\right) = V\beta_p \tag{2.16}$$

have the discontinuity. Beside the Ehrenfest classification, another division exists, namely on continuous or discontinuous phase transitions and this division is defined by the entropy's S behavior. So transitions where the entropy is continuous/discontinuous are classified accordingly. Therefore I order transitions are discontinuous, while e.g. II order transitions are continuous.

The enthalpy change ΔH at the phase equilibrium ($\Delta G = 0$) is closely linked with the entropy change ΔS via the following relation

$$\Delta H = T_m \Delta S, \tag{2.17}$$

where T_m is the melting point and has therefore also an discontinuity. With the discontinuous enthalpy the material's heat capacity should have a divergent behavior at the phase transition (see Fig. 2.1). In real systems however this is not the case (see Fig. 2.2).

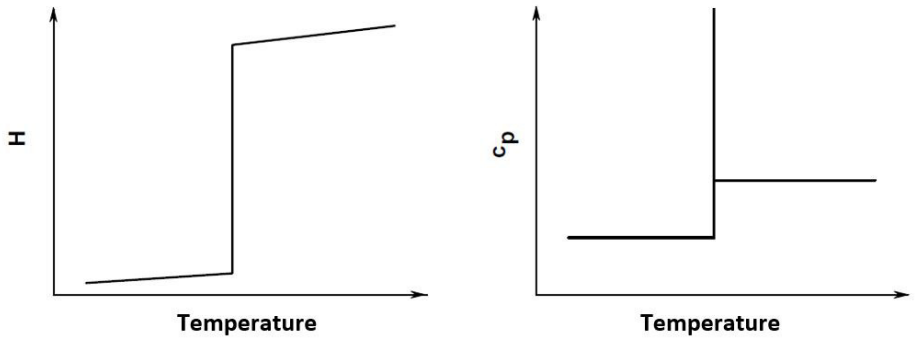

Figure 2.1: Schematic depiction of the enthalpy H (left) and specific heat capacity (right) near the melting point.

The first law of thermodynamics defines the relation between the internal energy and heat

$$dU = dQ - p \cdot dV. \tag{2.18}$$

For an isochoric process ($dV = 0$) a relation between the internal energy and the heat capacity can be derived.

$$dQ = c_V \cdot m \cdot dT = C_V \cdot dT \tag{2.19}$$

$$(dU)_V = dQ = C_V \cdot dT \tag{2.20}$$

$$C_V = \left(\frac{\partial U}{\partial T}\right)_V \tag{2.21}$$

If an isobaric process ($dp = 0$) is considered, a connection between the heat capacity and enthalpy can be established. One defines the enthalpy H as

$$H = U + p \cdot V. \tag{2.22}$$

The total differential gives the following result

$$dH = dU + dp \cdot V + p \cdot dV = dQ + V \cdot dp \tag{2.23}$$

For an isobaric process ($dp = 0$) one obtaines the following relation between the enthalpy and the specific heat capacity

$$(dH)_p = dQ = C_p \cdot dT. \tag{2.24}$$

From this it follows that the specific heat capacity is the partial derivative of the enthalpy with regards to the temperature

$$C_p = \left(\frac{\partial H}{\partial T} \cdot \right)_p \tag{2.25}$$

Calorimetric investigations are conducted with approximately constant pressure and therefore C_p is a very important quantity for calorimetry.

C_p and C_V are very similar for solids and fluids, because the volumetric expansion is minor. Significant difference between those two quantities appear in gaseous form.

In reality the I order phase transition is a continuous process. That means that the

specific heat capacity is not indefinite in this case at a melting temperature, but rather has a melting range where the property changes gradually [8, 18] (see Fig. 2.2).

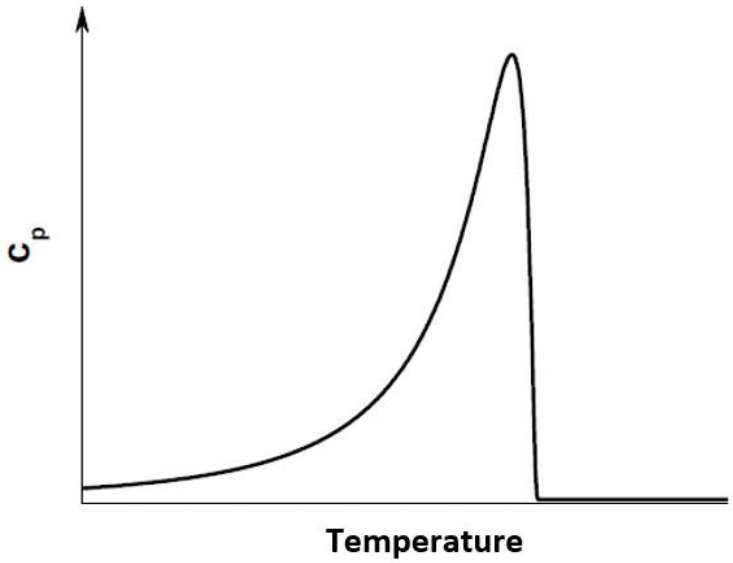

Figure 2.2: Apparent specific heat during a phase transition

This behavior is due to the fact, that the heat needs time to traverse the matter. The DSC process, during which the apparent specific heat curve is recorded, measures the temperature at the bottom of the crucible that contains the sample and thus overestimates the sample temperature. Due to the experimental set up of the DSC process, the measured heat capacity does not show the theoretically expected divergence, but it is rather the specific heat capacity of the system as a whole. Hence, in the DSC measurement the curve forms differ for different heating rates. The higher the heating rate the broader is the temperature range for the melting process and with it, the peak

of the specific heat during the transition.

2.3 Latent Thermal Heat Energy Storage

Thermal Energy Storages (TES) are part of highly integrated energy systems that can store energy for later purposes. They provide an effective way of storing thermal energy from various sources. TES can be operated with either sensible or latent heat. While TES driven by sensible heat do not utilize the advantage of phase transitions for storing energy, latent heat thermal energy storages (LHTES) use phase change materials (PCM) as medium to store latent heat (see Section 2.3.1) and therefore have two major advantages towards sensible heat TES. Firstly, PCMs provide a much higher thermal energy storage density than materials used in common TES, while requiring smaller masses and volumes of material [5]. This aspect increases the performance of these systems drastically. Secondly, due to it's isothermal nature, LHTES can accumulate energy with smaller temperature swings.

LHTES are used with renewable energy source to provide a more equal energy supply. A lot of renewable energy sources are intermittent and unpredictable. Often they depend on the weather and daytime, e.g. solar energy or wind turbines. One day they provide a great amount of energy, the other day almost none. For maximum efficiency it is indispensable to be able to store abundant energy for later use, thus LHTES are of so great importance. Numerous other applications for example are: building applications, thermal control applications in buildings and space crafts, off-peak electricity storage

systems and waste heat recovery systems. More details about them and other LHTES applications can be found in [6, 16, 19].

Currently, various practical problems arise in LHTES. During the phase change of the PCM problems like variation in thermo-physical properties under extended cycles, phase segregation, subcooling, irregular melting, volume change and high cost are encountered [2]. The problem that this thesis addresses, is the low thermal conductivity of the PCM. This results in a heating/cooling rate dependent transition temperature range and affects the performance of the LHTES. PCM with narrow melting temperature ranges are recognized to have better thermal performance, since it is easy to absorb or release latent heat [13].

2.3.1 Phase change materials

PCMs can store large amounts of energy with small temperature changes and therefore they are the essence of LHTES.

There is a wide range of different PCMs to choose from. Depending on the desired application, multiple PCMs with varying parameters (latent heat, melting/solidification temperature, phase change range, etc.) are available. They can be classified into 3 categories:

- organic
- inorganic
- eutectic

PCM	$\boldsymbol{T_m}$ [°C]	**h** $[\boldsymbol{kJ/kg}]$
Water-Ice	0	335
HD-PE	110 - 134	195,1
GR25	23,2 - 24,1	45,3
RT25 - RT30	26,6	232
n-Octadecane	27,7	243,5
Erythritol	117,7	339,8

Table 2.1: Thermophysical properties of several PCMs [1]

The high density polyethylene PCM used in the experiments which are evaluated in this thesis, belongs to the organic category. Table 2.1 lists a few PCM for the sole purpose of showing the difference in the crucial parameters between various PCMs. More details on other PCMs can be found elsewhere (see [1, 14, 15, 17]).

2.4 Differential Scanning Calorimetry

2.4.1 Fundamentals

In the differential scanning calorimetry (DSC) process the heat that is absorbed by or evolved from a sample is measured. Many phase transitions and chemical reactions are connected with generation or consumption of heat, i.e. are exothermic and endothermic processes. Therefore the DSC is used to investigate various materials and to analyse their thermal behavior. To avoid any possibility of confusion the difference between a DSC and a DTA (differential thermal analysis) should be pointed out. While a DTA measures the variation of the difference in temperature between the sample and

a reference sample, a DSC measures the variation of the difference in the heat flux [9]. The DSC is available in two designs:

- heat flux DSC
- power compensation DSC

The power compensation DSC measures the appearing difference in temperature between sample and reference sample and then compensates it by a corresponding change in heating power. While the differential heat flux then is exactly the difference in heating power, the heat flux DSC obtains the desired information indirectly through measuring the temperature difference. From this signal the heat flux can be obtained as follows

$$\dot{Q} = K(T) \cdot \Delta T \tag{2.26}$$

whereby K(T) is a calibration factor, which is found to be dependent on the temperature and can be determined through heat calibration/caloric calibration. This thesis will only discuss the heat flux DSC.

2.4.2 Heat flux DSC

Functional principle

The heat flux DSC's primary measurement signal is a voltage, received from the thermocouples beneath the crucibles. The crucibles used for holding the sample are shown

in Fig. 2.3. As shown in Fig. 2.4 these crucibles, which contain the sample and the reference sample, are placed in a cylindrical furnace and are subjected to a controlled temperature program. During this program (heating or cooling) the samples exchange heat with their surroundings.

Figure 2.3: Standard aluminium crucible

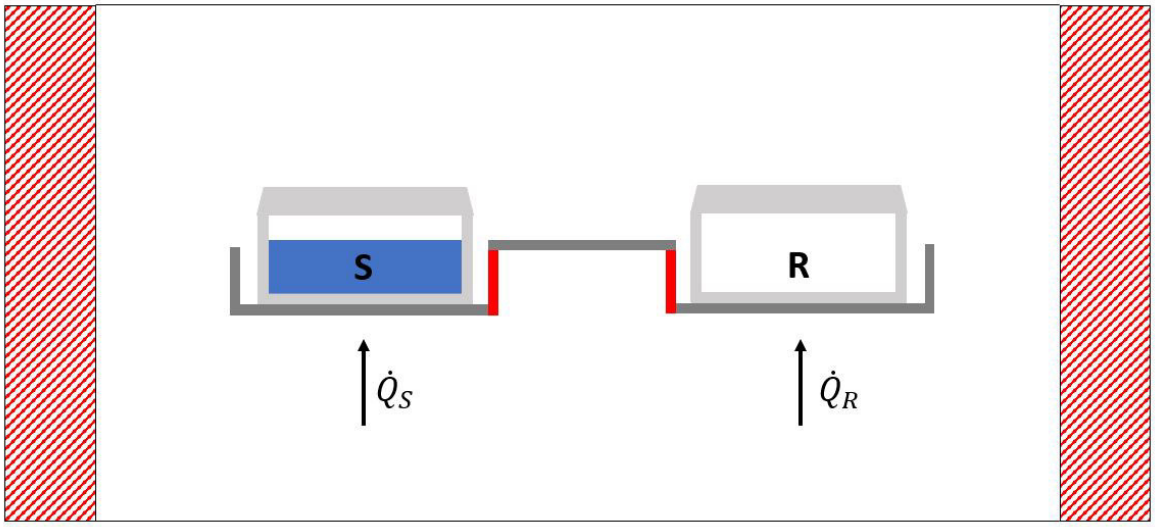

Figure 2.4: Schematic representation of a DSC furnace. The crucibles, including the lid are made of aluminium oxide (Al_2O_3). Both crucibles are placed on a holder. The heat flux between the samples via the holder is minimized through a material with low heat conduction. The assumption that the heat enters through the bottom is discussed in Section 2.5.

With the assumption of thermal symmetry (for empty crucibles the measured signal should be zero) and steady-state conditions, the difference between heat fluxes can be described as follows:

$$\begin{aligned} \dot{Q}_{Left} - \dot{Q}_{Right} &= (\dot{Q}_S + \dot{Q}_{Crucible}) - (\dot{Q}_R + \dot{Q}_{Crucible}) = \\ \dot{Q}_S - \dot{Q}_R &= k \cdot A \cdot (T_{Furncace} - T_S) - k \cdot A \cdot (T_{Furncace} - T_R) = \\ &K \cdot (T_S - T_R) = K \cdot \Delta T(t) \end{aligned} \tag{2.27}$$

Because the reference side is empty, the heat flux equals zero and the relation above is obtained [11]

$$\dot{Q}_S = K(T) \cdot \Delta T(t). \tag{2.28}$$

The factor $K(T)$ can be determined using calibration materials whose thermodynamic properties are well-known. This process will be discussed later in Section 2.4.2.

Temperature calibration

The temperature measured via the thermocouple is not exactly equal to the prevailing temperature of the sample. This is due to the fact that between the sample and the thermocouple the crucible itself and the crucible holder are located, which results in an inevitable temperature difference. In addition, it is also possible that the thermocouples are not perfectly calibrated. To be able to obtain the correct temperature in the reference crucible, it is a must to conduct a temperature calibration. The correction has to be done separately for every heating rate, because higher heating rates lead to larger temperature gradients and therefore result in a larger discrepancy between the measured and the actual temperature.

The temperature calibration is done with the help of calibration substances with well-known melting temperatures. To receive a very accurate calibration curve for a broad temperature range it is necessary to utilize several calibration substances. More information on this subject is provided in [9].

Caloric calibration

As mentioned above, the heat calibration is a necessity to determine the calibration constant $K(T)$ and thus the heat flux that entered the sample (2.28). There are several methods to carry this out, but this thesis will only cover the *heat peak area calibration* because the used apparatus uses this method [9].

As for the temperature calibration, materials with well-defined heat of transition - so called calibration materials - are required for this process. By measuring the area under the DSC signal corresponding to a phase transition, a phase transition heat can be assigned to the material. After comparing this measured heat with the value from the literature, the calibration factor can be calculated. The factor is temperature-dependent and therefore several substances are needed to obtain a more precise function for a broad temperature range (see Fig. 2.5).

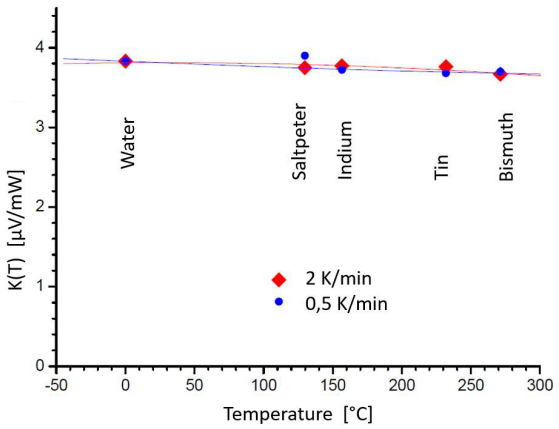

Figure 2.5: Caloric calibration: with the help of well-known Standards *(Certified Reference Materials)* a function for the calibration coefficient is obtained.

DSC Measurements and curves

The original measurement signal is a voltage in the µV-range which then is transformed into the temperature difference between the sample and reference sample. The sample temperature lags behind the reference temperature ($T_R > T_S$). During a first order phase transition, the sample temperature remains constant, until the phase change is completed. The characteristic curve is thus formed (see Fig. 2.6).

The temperature difference then is transformed into various quantities - normally the heat flux - and the latter is plotted versus the time or a temperature. This plot is typical for DSC measurements (see Fig. 2.7).

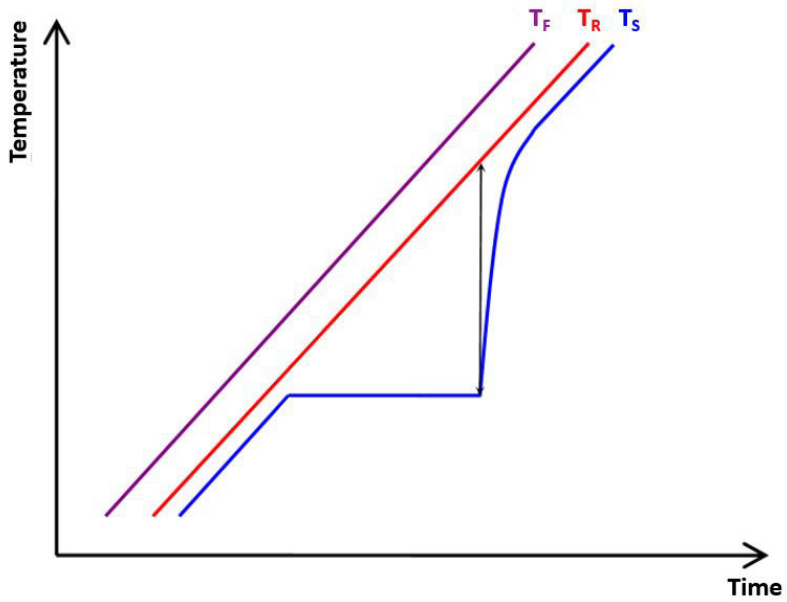

Figure 2.6: Temperatures in a DSC: T_F represents the furnace temperature (violet), T_R represents the reference temperature (red), T_S represents the sample temperature (blue). Because of the phase transition T_S lags behind the reference.

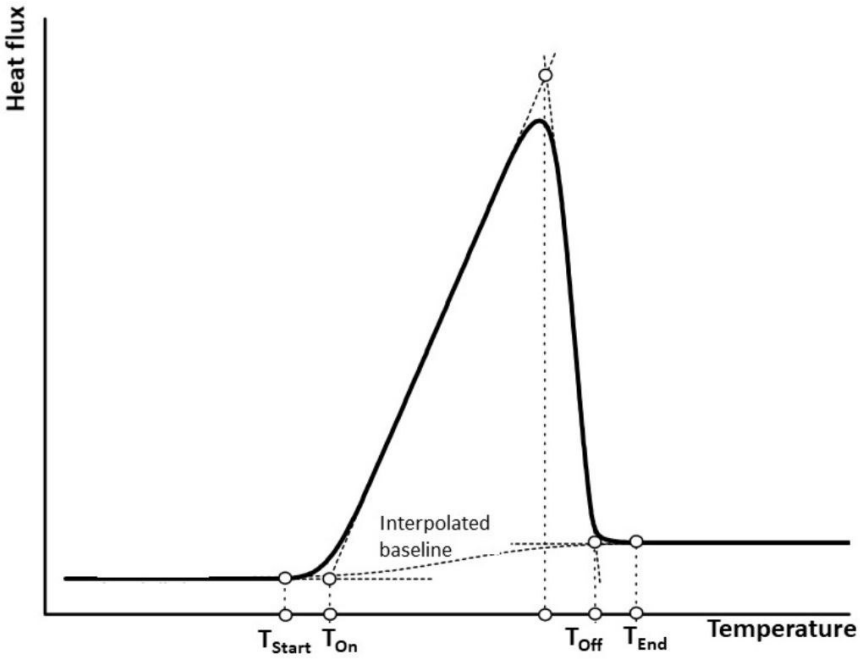

Figure 2.7: Depiction of a DSC curve: T_{Start} represents the beginning of the phase transition, T_{End} represents the end of the phase transition, T_{On} and T_{Off} represent the basis for calculating the interpolated baseline.

This curve shows four different temperature values. While T_{Start} and T_{End} indicate the beginning and ending of the transition process of the material, the onset and offset temperatures represent the extrapolated starting and ending temperatures of the process. Furthermore, the onset temperature marks the point at which the melting of the main phase starts. This difference between T_{Start} and T_{On}, that can be observed in DSC measurements, is the subject of this thesis's topic. In contrary of what is to be expected when a phase transition starts, the immediate start of the melting process (T_{Start} and T_{On} should overlap) is not being observed. On the contrary, the phase change is pre-

luded with a slight slope of the curve, followed by a rapid increase of the heat flux at the onset temperature. Therefore, the onset temperature is utilized as a reference point. The onset and offset temperatures can be obtained via various methods. One acknowledged method is the intersection of auxiliary lines in the peak area with the extension of the pre-transition baseline.

The reason for the shift of the melting temperature to the onset temperature is the fact, that polymeric systems are not solely made of one certain chain length but rather consist of multiple chain lengths and each one has a different melting temperature. With a certain distribution of chain lengths the polymer then has a specific delay that is observed during a DSC measurement [7].

The term baseline depicts the DSC curve before and after the phase transition. It is formed by the heat flux into the sample and the zero line. The zero line is the curve without a sample, subjected to the same temperature program to embrace all occurring asymmetries of the measuring device. To obtain the real heat flux into the sample, the corresponding zero line has to be subtracted from the measurement.

So, before any measurement, the zero line must be determined. This curve afterwards is subtracted from the sample measurement, so that all the asymmetries of the DSC are faded out. Moreover, also the temperature and heat calibration must be performed to correct the measurement. The actual measurement is conducted with one crucible filled with the sample and the other with a reference sample (often empty). The recorded curve then represents the real heat flow consumed/produced by the sample.

2.4.3 DSC Apparatus - *DSC 204 F1 Phoenix*

For the measurements conducted at the Austrian Institute of Technology, a device from *NETZSCH-Gerätebau GmbH* - the DSC 204 F1 Phoenix was used. This apparatus is a heat flux DSC with an automated sample changer. The furnace consists of a cylindrical high-conductivity silver block with an embedded heating coil for thermal symmetry in the sample chamber (see Fig. 2.10).

With it's disk-shaped silver carrier plate and supersensitive thermosensors of nickel-chromium constantan (type E thermocouples), the sensor offers a high level of calorimetric sensitivity (see Fig. 2.11).

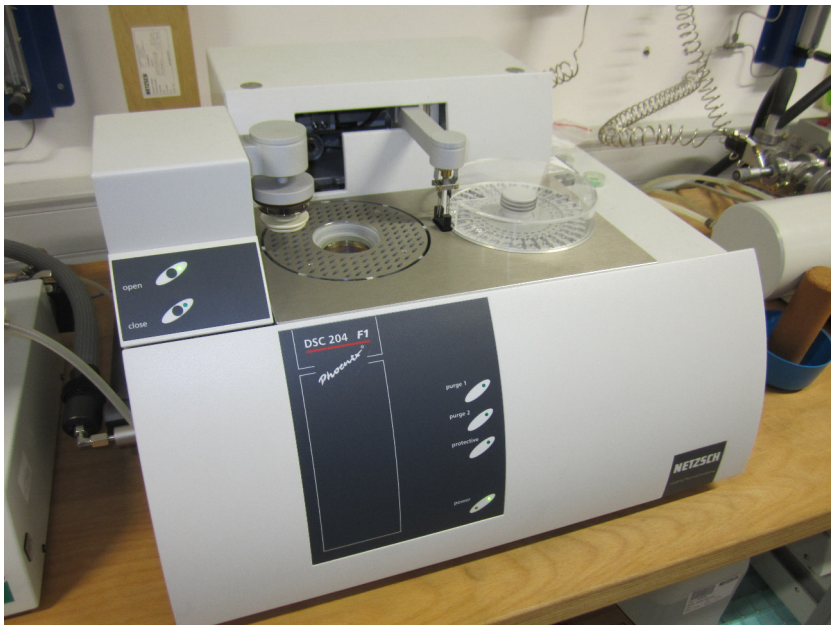

Figure 2.8: DSC 204 F1 Phoenix - front view

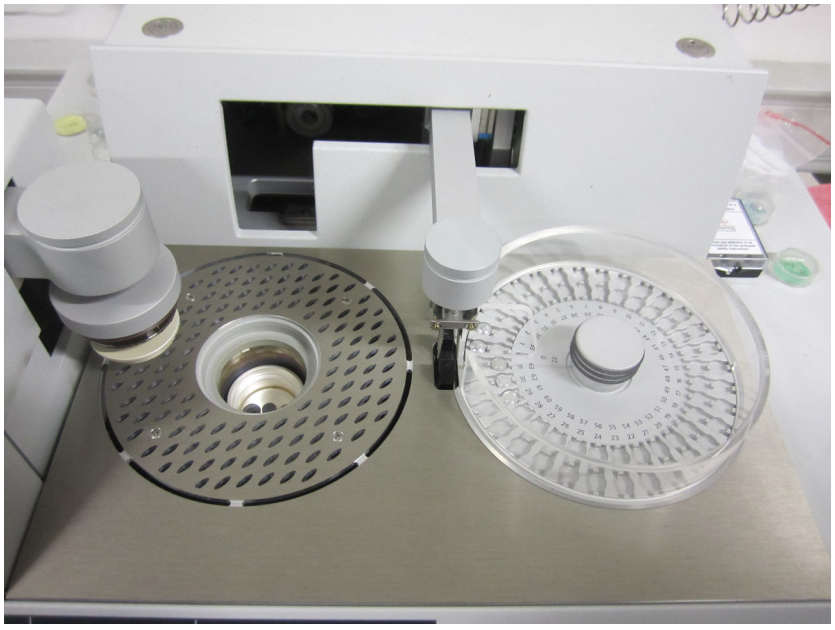

Figure 2.9: DSC 204 F1 Phoenix - top view

Figure 2.10: DSC 204 F1 Phoenix - furnace

Figure 2.11: DSC 204 F1 Phoenix - holder with sensor

Thermocouples

A thermocouple consists of two different wires, which are connected to each other at one end. At the other end of the wires a temperature-dependent voltage occurs due to the thermoelectric effect, which is then converted to temperature (see Fig. 2.12).

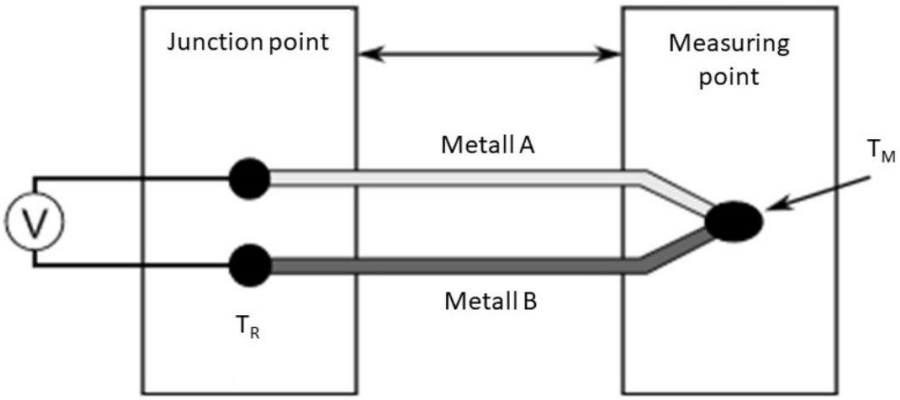

Figure 2.12: Schematic representation of a thermocouple

When the temperature at the measuring point is different to the reference temperature at the junction point, the temperature difference is given by

$$\Delta T = T_M - T_R = \frac{U}{S(T)} \tag{2.29}$$

$S(T)$ is the temperature-dependant Seebeck coefficient. Depending on what type of thermocouple is used (varying wire materials), one can conduct a transformation with the help of the electrochemical series (see App. D).

In Fig. 2.13 and Fig. 2.14 the sensor used in the DSC 204 F1 Phoenix is depicted.

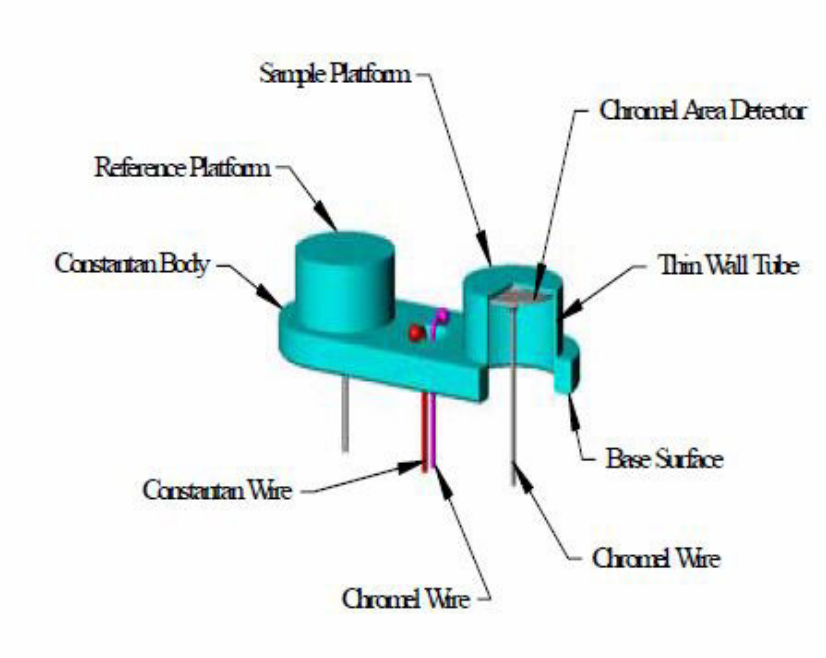

Figure 2.13: DSC Sensor - detailed sketch

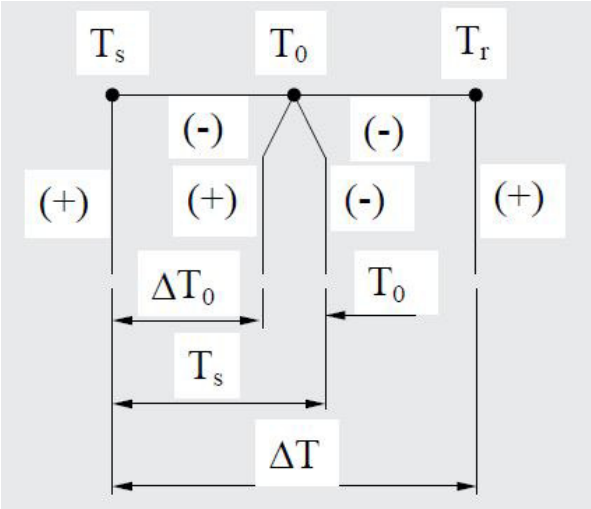

Figure 2.14: Sensor sketch

2.5 Model

In this section a model for the DSC process is outlined and discussed for a continuous heating process. The motivation for establishing this model is to be able to conduct a numeric simulation of the sample temperature during the DSC process. The goal of the numeric simulation is to determine the specific heat of the PCM through comparing the measured and simulated sample temperature. Then with the help of the Matlab integrated non-linear least square method, a parameter fitting can be realized.

The geometry of the sample in the crucible is depicted in Fig. 2.15.

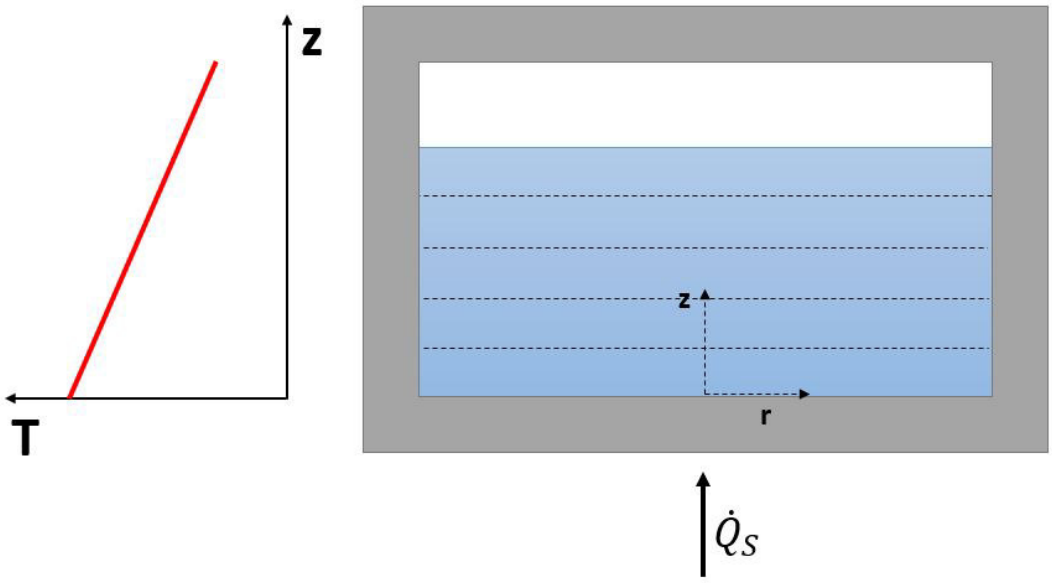

Figure 2.15: Geormetry of sample crucible: $H << R$. The red line depicts the temperature profile alongside the z-axis of the cylindric sample.

It is assumed that the only heat transport mechanism is heat conduction. Because of the low temperature range in which the process occurs the radiation is neglected. Due to the small size of the crucibles the convection effects are also not considered. The simulation is based on a planar one-dimensional model. It presumes that the whole heat enters the sample through the bottom side of the crucible. This assumption is justified by the sample geometry. Because the sample height is much less than the sample diameter ($H << 2R$), the contact side surface between crucible and sample is much smaller than the bottom surface. Furthermore, the heat flux from the sample top surface is neglected, because the heat conductivity of the air is a lot smaller than the heat conductivity of aluminium oxide. The heat that enters the sample then is conducted in axial direction without losses through the crucible wall, resulting in a temperature gradient alongside only the z-axis. For simulating the heat conduction in axial direction, it is necessary to discretize the sample. Discretization is obtained using the central difference quotient (see Section 3.1.1).

The data provided by the DSC experiment are the voltage signal, the corresponding sensitivity values (S) and the reference temperature. With the sensitivity curve the voltage can be transformed into the heating power that enters the sample

$$[\dot{Q}] = \frac{[U]}{[S]} = \frac{\mu V}{\frac{\mu V}{mW}} = mW. \tag{2.30}$$

Through the discretization of the sample it is possible to utilize the heat to obtain the temperature outside the sample. With the following initial and boundary conditions

Eq. 2.12 can be solved.

$$\frac{\partial T}{\partial r}(t,r,z)\Big|_{r=R} = 0 \tag{2.31}$$

$$\frac{\partial T}{\partial z}(t,r,z)\Big|_{z=H} = 0 \tag{2.32}$$

$$\frac{\partial T}{\partial z}(t,r,z)\Big|_{z=0} = T_{crucible} \tag{2.33}$$

$$T(t,r,z)\Big|_{t=0} = T^0(r,z) \tag{2.34}$$

With Eq. 2.33 a boundary condition T_{N+1} is obtained and can be used as input for the simulation. T_{N+1} - which is the temperature of the crucible bottom ($T_{crucible}$) - is received via Fourier's law

$$\dot{q} = \lambda \frac{T_{N+1} - T_N}{\Delta z} \tag{2.35}$$

$$T_{N+1} = \frac{\dot{q}}{\lambda}\Delta z + T_N \tag{2.36}$$

whereas the temperatures T_i refer to the temperatures of every infinitesimal sample segment, λ is the heat conductivity of the sample and Δz is the size of the numerical grid (see Sec. 3.1.2).

For the discretization parameters the following values were used

2.6 Properties of Sapphire

The model presented in Sec. 2.5 first needs to be validated with a material that has well-known thermophysical properties. In this case the model is examined with a sapphire, declared as a standard by the National Bureau of Standards (see App. A).

Specific heat capacity

Sapphire's specific heat capacity is exactly measured over a wide temperature range and the temperature dependence is fitted by a polynomial of high order

$$c_p(T) = \sum_{i=0}^{10} A_i x^i \tag{2.37}$$

whereby the temperature is transformed to $x = \dfrac{T_K - 650}{550}$ (T_K annotates that the temperature value is in Kelvin). The parameters are determined as follows

- $A_0 = 1,12705$
- $A_1 = 0,23260$
- $A_2 = -0,21704$
- $A_3 = 0,26410$
- $A_4 = -0,23778$
- $A_5 = -0,10023$
- $A_6 = 0,15393$
- $A_7 = 0,54579$
- $A_8 = -0,47824$
- $A_9 = -0,37623$
- $A_{10} = 0,34407$

The original documentation can be found in App. E.

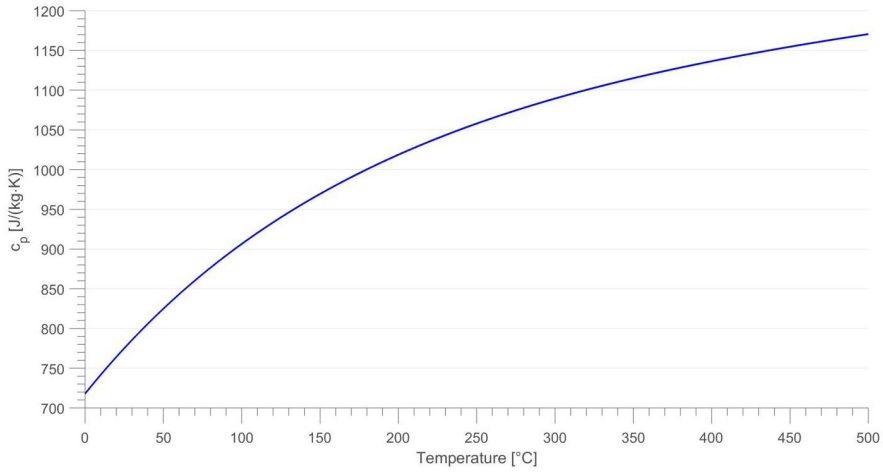

Figure 2.16: Specific heat capacity for Sapphire ($\alpha - Al_2O_3$)

Thermal conductivity

For the simulation of the heat conduction through the sample another essential property is necessary - the thermal conductivity. However, for the simulation the thermal conductivity of the polycrystalline sapphire was used, because the data of monocrystalline sapphire was not available in literature. A few values for different temperatures were found in the database of the *Netzsch software*. Therefore the data were extrapolated with a polynomial of second order

$$\lambda(T) = A_0 + A_1 \cdot T_K + A_2 \cdot T_K^2 \tag{2.38}$$

The temperature T_K is given in Kelvin and the parameters are determined as follows

- $A_0 = 91.64061$
- $A_1 = -0.28297$
- $A_2 = 0.00027$

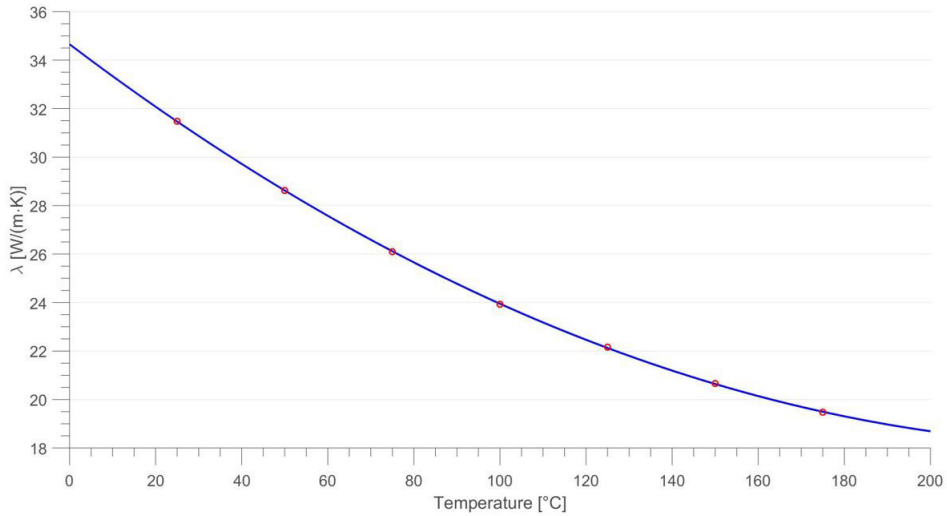

Figure 2.17: Thermal conductivity for polycrystalline Sapphire ($\alpha - Al_2O_3$)

Density

Furthermore, to be able to conduct a DSC Simulation, the materials density is necessary. In the temperature range in which the experiment is conducted, the sapphire's density has an almost constant value of $\rho = 3970 \frac{kg}{m^3}$.

Methods

At the beginning of this chapter the details of the simulation techniques are discussed, such as numerical methods and boundary conditions. Furthermore, the result of the simulation with the sapphire is conducted and analysed.
Finally, the simulation is carried out for a polymer, with a parameter fitting procedure to determine the "apparent" specific heat capacity.

3.1 Simulation

3.1.1 Numerical Methods

Eq. 2.10 is simplified if we assume that rotational symmetry is given. Moreover, conduction in the radial direction is neglected for now, because it is assumed, that the heat enters the sample uniformly from below. Therefore one obtains [2]

$$\boxed{\rho c_p \frac{\partial T}{\partial t} = \frac{\partial}{\partial z}\left(\lambda \frac{\partial T}{\partial z}\right)} \tag{3.1}$$

Hence the simulation is made in one dimension - in the axial direction. For the simulation of the heat conduction in the sample a discretization is obtained by using a central difference quotient [10, 2]. It is necessary to discretize the temperature field in space and time

$$T(z_j, t_k) = T_i^k. \tag{3.2}$$

With this procedure one can write the second derivative as follows

$$\left(\frac{\partial^2 T}{\partial z^2}\right)_i^k = \frac{T_{j-1}^k - 2T_j^k + T_{j+1}^k}{\Delta z^2} + \mathcal{O}(\Delta x^2) \tag{3.3}$$

as well as the time derivative

$$\left(\frac{\partial T}{\partial t}\right)_i^k = \frac{T_j^{k+1} - T_j^k}{\Delta t} + \mathcal{O}(\Delta t) \tag{3.4}$$

With these simplifications the spatial part of the ordinary differential equation (ODE) evaluates to the following

$$D = \frac{\partial}{\partial z}\left(\lambda \frac{\partial T}{\partial z}\right) \tag{3.5}$$

$$D_j = \frac{1}{\Delta z}\left[\frac{\lambda_{j+1/2}}{\Delta z}(T_{j+1} - T_j) - \frac{\lambda_{j-1/2}}{\Delta z}(T_j - T_{j-1})\right] \tag{3.6}$$

with

$$\lambda_{j\pm 1/2} = \frac{2\lambda_i \lambda_{i\pm 1}}{\lambda_i + \lambda_{i\pm 1}} \tag{3.7}$$

being the harmonic mean. With the use of the central difference quotient the ODE can finally be simplified to the following discretized term

$$\frac{\partial T_j}{\partial t} = \frac{D_j}{\rho_j c_j} \tag{3.8}$$

The spatial part of the ODE, D_j was solved manually and integrated in the Matlab code, while the time derivative was solved via a Matlab-integrated ODE-solver. The used ODE-solver was the *ode15s*, which is used to solve stiff differential equations. The simulation was carried out with a grid size of $N = 100$, which resulted into a mesh size of $dz = 5,75\mu m$.

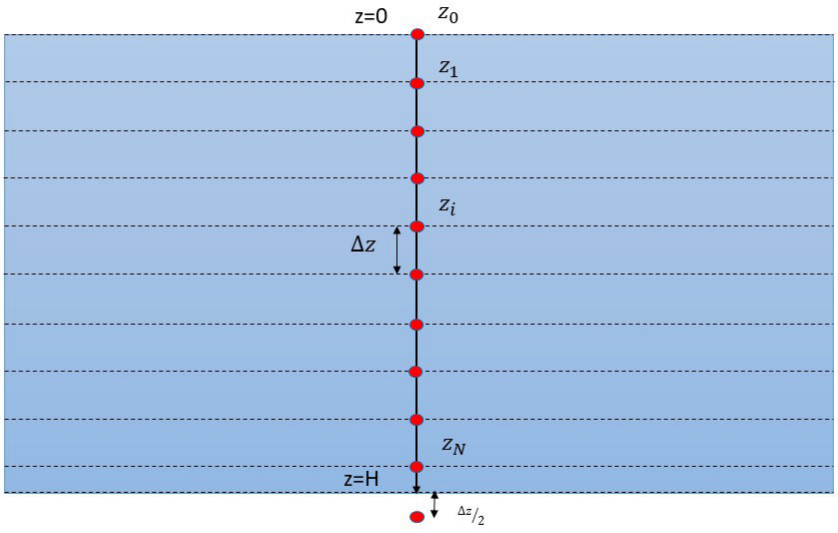

Figure 3.1: Discretization grid: the sample is viewed as an concatenation of infinitesimal disks along the z-axis

3.1.2 Grid

For a successful simulation a suitable grid is a necessity. For this problem the grid is chosen in a way that a node is outside the sample in a distance of $\frac{\Delta z}{2}$ (see Fig. 3.1). The reason for this is the nature of the input parameter. Due to the heat being the simulation's input, it is inevitable to place a node outside the sample. With this trick it is possible to define a boundary condition via a temperature gradient (see Sec. 3.1.3).

3.1.3 Boundary and initial conditions

After describing the materials properties, discretizing the differential equation and defining a grid it is time to determine boundary conditions.

Initializing the temperature profile

At the start of the simulation a temperature profile throughout the sample is necessary. To realize this, the temperature at the sample bottom ($T\Big|_{z=H}$) is calculated. This is done with the knowledge of the measured reference temperature T_R, the DSC-signal U and the electrochemical series of the thermocouple (see App. D). Since the thermal conductivity of the sample is known, the initialization of the rest of the sample is done with Fourier's law.

Boundary conditions

To provide the simulation with data, boundary conditions are essential. For that matter $T(z_{N+1}) = T_{N+1}$ needs to be established. The model assumes that the heat enters the sample only from the bottom of the crucible. Therefore the following boundary condition is obtained

$$T_{N+1} = \frac{\dot{q}}{\lambda}\Delta z + T_N \tag{3.9}$$

As input the heat flux $\dot{q}$ is used to simulate the boundary temperature. With the help of a Matlab integrated ODE-solver the heat conduction equation is solved and the remaining temperature profile can be calculated.

Results

4.1 Simulation of the DSC process with a Sapphire

4.1.1 Measurement

The measurement series with the sapphire ($\alpha - Al_2O_3$) was conducted for the following sample masses:

- $m_1 = 21,09mg$
- $m_2 = 42,15mg$
- $m_3 = 63,66mg$
- $m_4 = 84,73mg$

Each sample was subjected to several heating-cooling cycles that were interrupted by a 5 minute long isothermal segment (see Fig. 4.1). While the cooling segments were performed with a rate of $\beta = 10K/min$, the heating segments were carried out with a geometric declining rate ($\beta \in [20; 10; 5; 2.5; 1.25]$).

Fig. 4.2 shows the heating curves of the sapphire measurement series in the form of a voltage signal. Except one heating segment, which contains an measurement artifact that can be traced back to the involved equipment, all curves are used to test the DSC model that was described in Section 2.5.

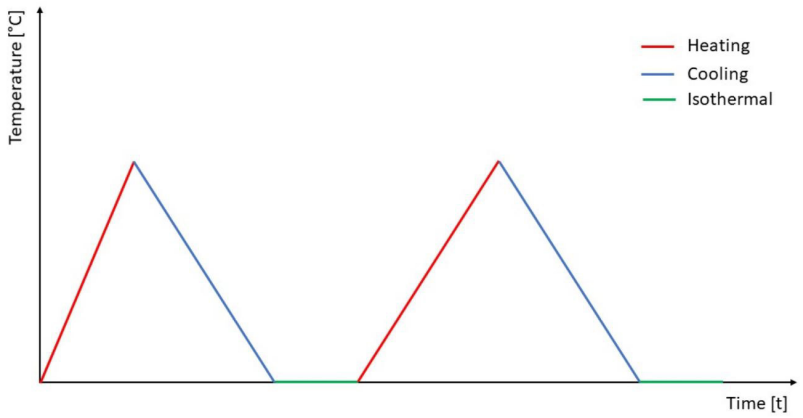

Figure 4.1: DSC measurement program - Red: heating segments with a geometric declining heating rate. Blue: cooling segments with one cooling rate of 10K/min. Green: isothermal segments to establish thermodynamic equilibrium.

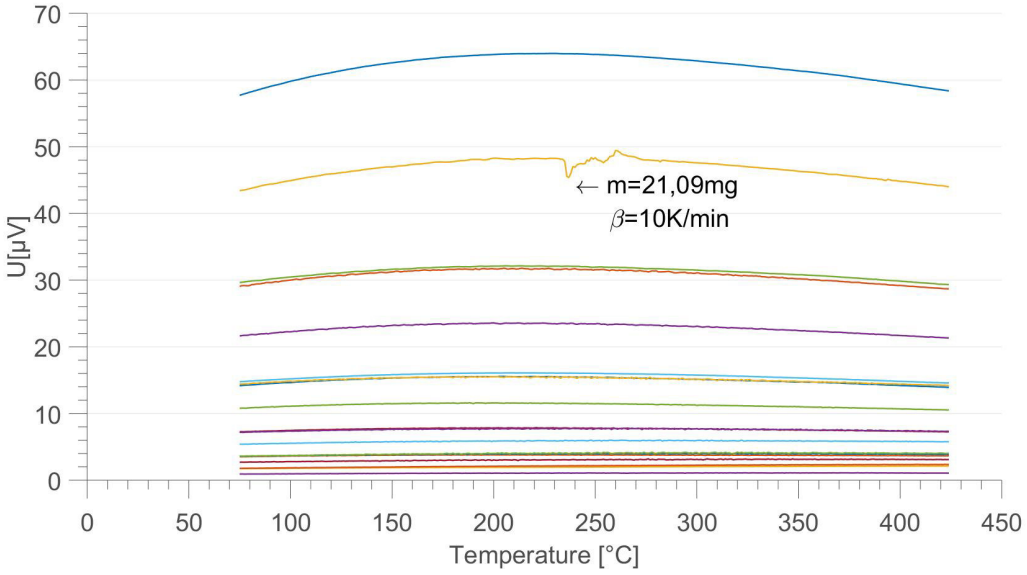

Figure 4.2: Sapphire measurement series - Voltage signal from DSC measurement for the heating curves. One measurement artifact is present for the sample mass $m = 21,09mg$ at the heating rate $\beta = 10K/min$

Calibration curves

The calibration curves were analysed and compared to the mean value and the standard deviation in Fig. 4.3. It can be seen that the curves, except one rogue result (sample mass of $21,09mg$ with a heating rate of $2,5K/min$), are within a certain scatter band. The curves show no clear dependence on mass or heating rate.

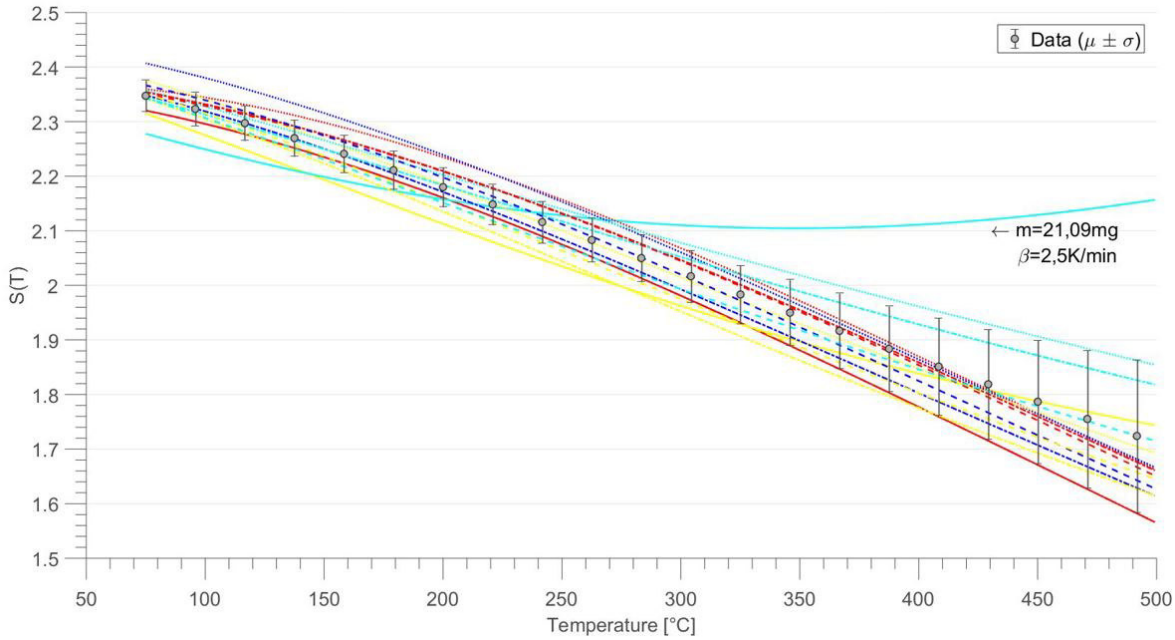

Figure 4.3: Sapphire - calibration analysis

The sensitivity curves are calculated internally in the *Netzsch software* via the following function

$$S(T) = (p_2 + p_3 \cdot z + p_4 \cdot z^2 + p_5 \cdot z^3) \cdot e^{(-z^2)} \tag{4.1}$$

with $z = (T_R - p_1)/p_1$ being a transformation of the reference temperature.

A second method for determining the sensitivity is directly through the DSC signal

$$S(T) = \frac{U(T)_{DSC,Standard} - U(T)_{DSC,Baseline}}{m_{Standard} \cdot c_p(T)_{Standard} \cdot \beta} \tag{4.2}$$

Both methods provide similar results, which suggests that the calibration curves are valid.

4.1.2 Simulation findings

Fig. 4.4 provides the result of the simulation for one sapphire sample. It depicts the difference between the simulated and the measured sample temperature for the sample of $m = 21,09mg$. The heating curve with a rate of $\beta = 10K/min$ was left out because of the artifact mentioned above. Furthermore, the curves with a rate smaller than $\beta = 2,5K/min$ produce unsatisfying results with unacceptable deviations from the real sample temperature (see Table 4.1.2). This can be traced back to the faint signal, which causes a bad signal-to-noise ratio. The rest of the simulation results are available in the App. F.

All together the simulation yields reasonable results with only slight deviations from the actual values. These findings imply the validity of the modelling of the DSC process.

β	m_1	m_2	m_3	m_4	
20	0,29 %	0,34 %	0,23 %	0,31 %	
10	0,21 %	0,28 %	0,25 %	0,28 %	
5	0,15 %	0,32 %	0,22 %	0,36 %	
2,5	0,18 %	0,33 %	0,33 %	0,29 %	
1,25	44,2 %	43,4 %	44,4 %	44,1 %	

Table 4.1: Relative error $\frac{\Delta T}{T}$ for all measurements

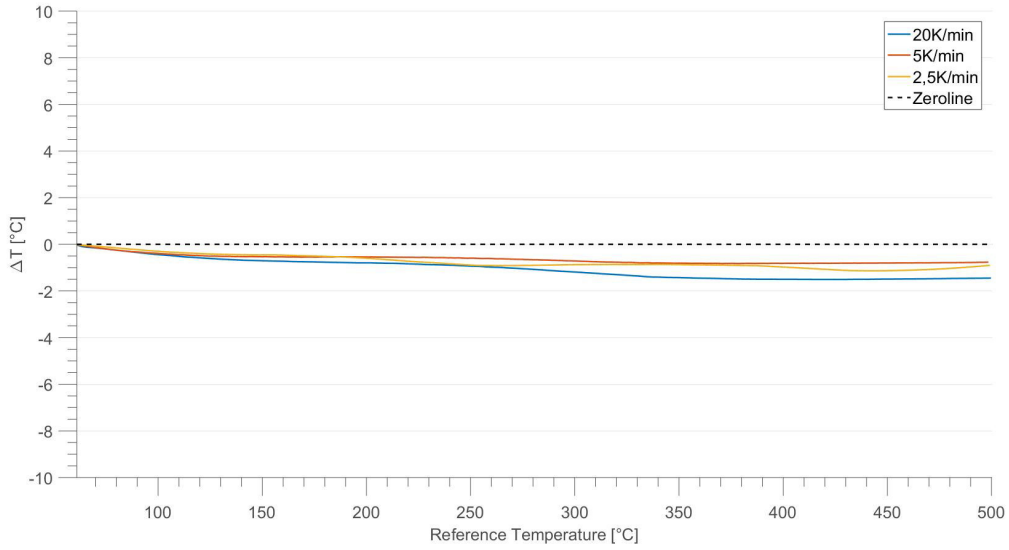

Figure 4.4: Difference between the simulated and the measured sample temperature for the sample of $m = 21,09mg$

4.2 Simulation of the DSC process with a PCM

4.2.1 Measurement

The measurement series with the phase change material was conducted for a sample with a mass $m = 10,47mg$. The sample was subjected to the same heating program as the sapphire one (several heating-cooling cycles with the cooling rate β (as follows) that were followed by a 5 minute long isothermal segment).

- $\beta = 20K/min$
- $\beta = 10K/min$
- $\beta = 5K/min$
- $\beta = 2,5K/min$
- $\beta = 1,25K/min$

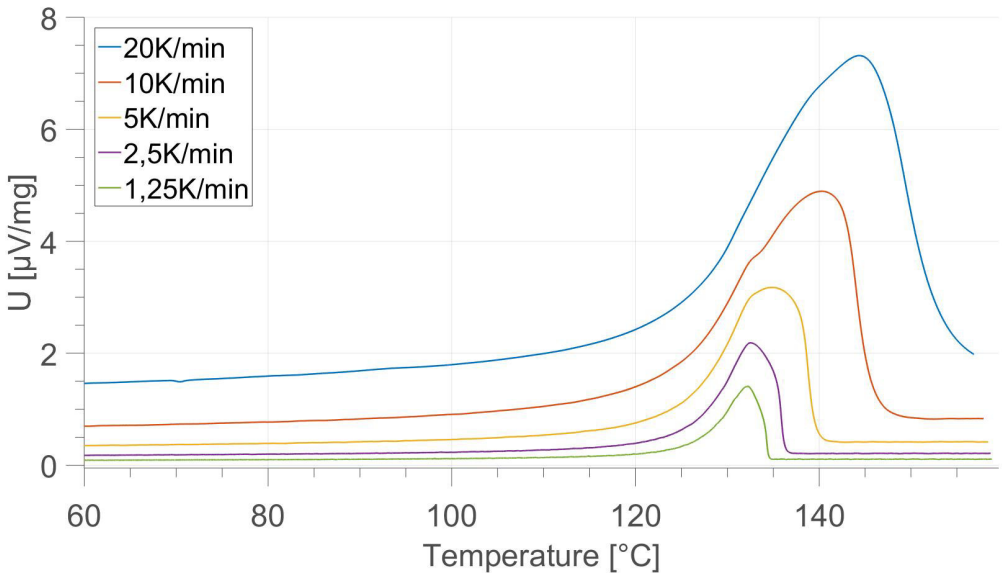

Figure 4.5: PCM measurement series - Voltage signal from DSC measurement for the heating curves

Fig. 4.5 shows the raw measurement data of a PCM sample for several heating rates. For the purpose of analysing and treatment of the melting process for all heating rates in a comparable way, the measurement curves were normalized to same height (see Fig. 4.6). In the figure, the starting points of the melting process are also depicted. The melting (or starting) temperature was set as the one at which a 5% of the signals maximum deviation from baseline was reached.

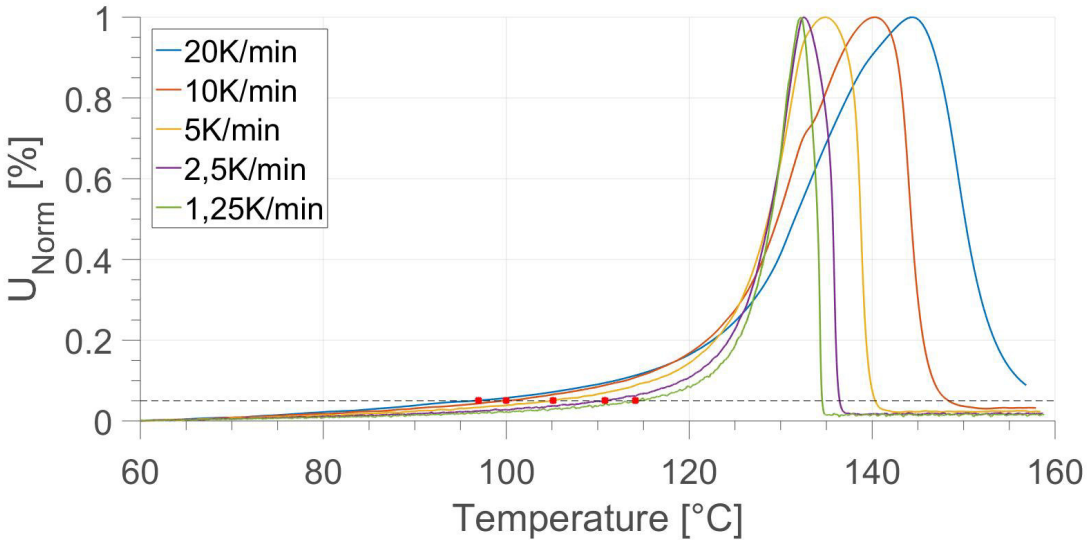

Figure 4.6: PCM measurement series - Normalized voltage signal. The dashed black line marks the 5 % as definition of the start of the melting process. The red dots denote the melting point for each curve.

Fig. 4.7 shows the onset temperatures T_{On} for each cycle. The calculation of the onset temperatures were done with the method described in Section 2.4.2. In this section the onset temperature is defined as extrapolated start temperature of the melting process. Table 4.2 lists all values of the starting temperatures T_{Start}, the onset temperatures T_{On}

and the difference ΔT between those two.

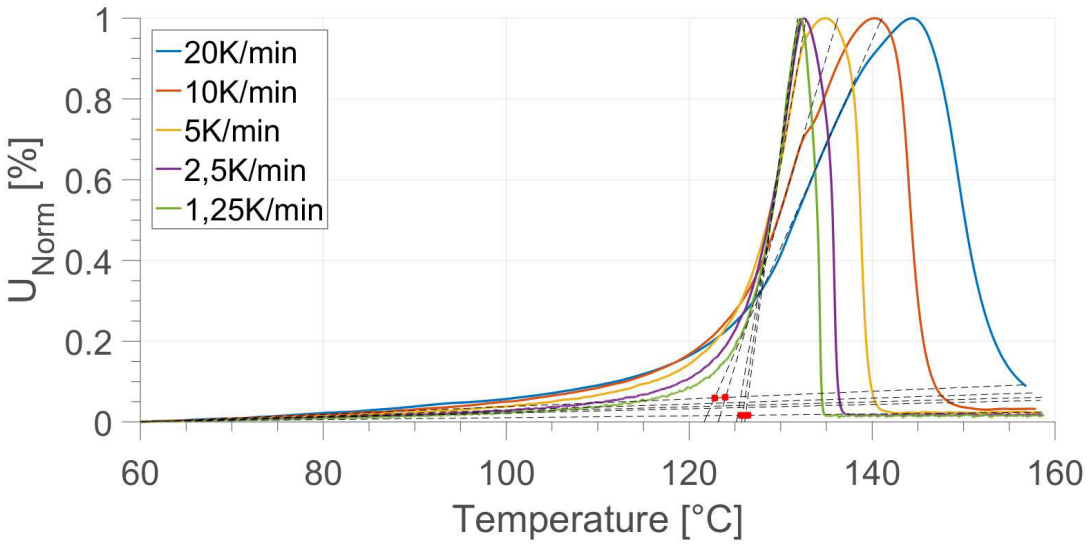

Figure 4.7: PCM measurement series - Normalized voltage signal with determined onset temperatures marked by the red dots.

$\boldsymbol{\beta}$ [K/min]	$\boldsymbol{T_{Start}}$ [°C]	$\boldsymbol{T_{On}}$ [°]	ΔT
20	96,94	122,8	25,26
10	100,02	123,9	23,88
5	105,1	125,7	20,6
2,5	110,76	126,2	15,44
1,25	114,08	126,4	12,32

Table 4.2: Characteristic temperatures

In Fig. 4.6 it can be seen that the start of the melting process differs for different heating rates. The determined values in Table 4.2 exhibit that the melting process start (starting and onset temperature) shifts to higher temperatures with decreasing heating rates. Column ΔT reveals the heating rate dependency of the delay of the melting process. For lower heating rates the delay decreases rapidly. The reason for this

phenomenon is the heat conduction. For infinitesimal heating rates the matter would always be in thermodynamic equilibrium and thus there wouldn't be any noticeable delay.

Measured specific heat capacity

From the measured curves the experimental specific heat capacity can be obtained via the integration method [1] (see Fig. 4.8).

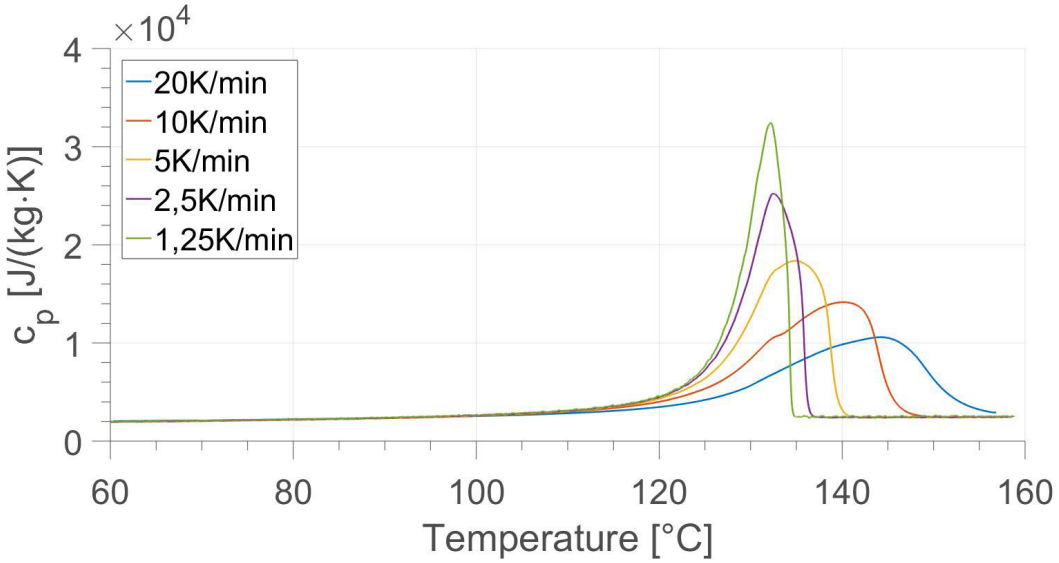

Figure 4.8: PCM measurement series - specific heat capacity obtained via integration method.

If the specific heat capacity curves are normalized and evaluated, similar values are obtained for the characteristic temperatures. This shows that the delay is also clearly visible in the specific heat capacities, measured by the integration method.

[1] The *integration method* is a way of calculating the specific heat capacity from the measured data by integrating the heat over time and then differentiating the result with respect to the temperature.

4.2.2 Thermal properties

The essential physical quantities used for the simulation of heat conduction through the polymer are listed below

- density ρ
- thermal heat conductivity λ
- specific heat capacity c_p

Experimental data for the density and the thermal conductivity are available from the Austrian Institute of Technology obtained via parameter fitting [2] of the data.
Both, the density as well as the heat conductivity of the polymer are represented with the following function

$$f(T) = \frac{c_1}{1 + e^{c_4(T-c_2)}} + c_3 \tag{4.3}$$

	$\boldsymbol{\rho}$	$\boldsymbol{\lambda}$
c_1	167.2182	0.41857
c_2	129.9861	265.5994
c_3	760.8218	0.5414
c_4	0.078916	0.0367

Table 4.3: Parameter sets for the PCM's density and thermal conductivity

With these parameters one obtains the density ρ in $[kg/m^3]$ (Fig. 4.9) and the thermal conductivity in $[W/(m \cdot K)]$ (Fig. 4.10).

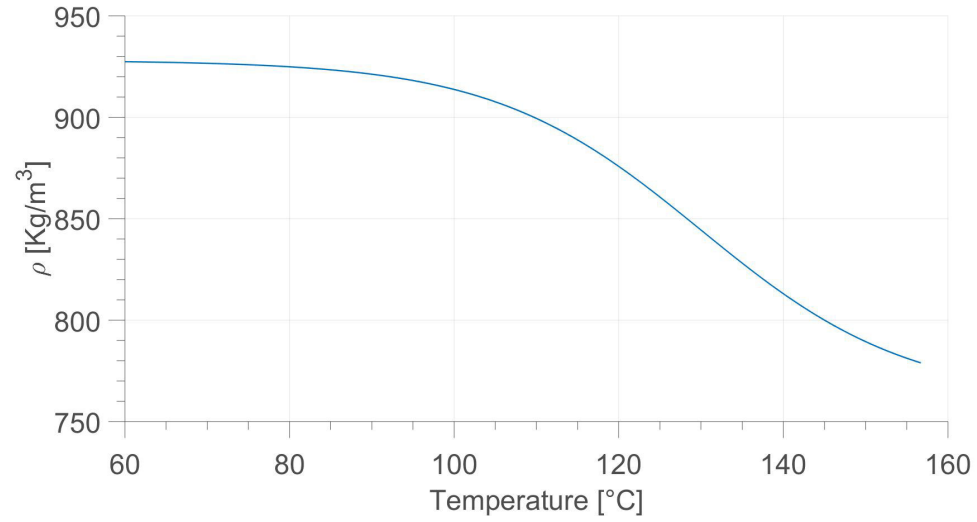

Figure 4.9: Temperature dependence of the density of the PCM

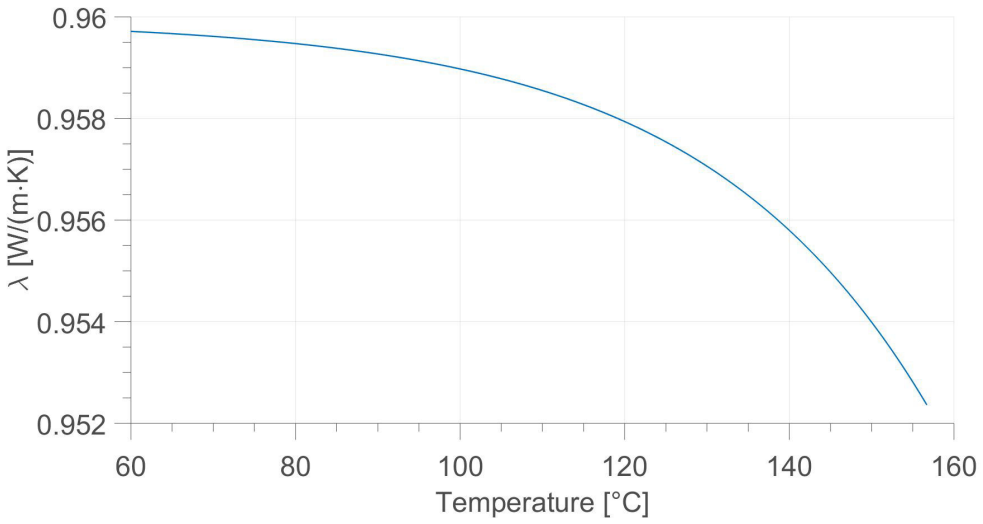

Figure 4.10: Temperature dependence of the thermal conductivity of the PCM

The apparent specific heat capacity on the other hand is to be determined. In the region of the phase transition it is being modelled with the Gumbel distribution, which is typically used to model the distribution of the maximum or minimum of phenomena. The Gumbel distribution is an *extreme value type I distribution*.

$$f(T) = \frac{1}{\beta} e^{\frac{x-\mu}{\beta}} \cdot e^{-e^{\frac{x-\mu}{\beta}}} \tag{4.4}$$

where μ is the location parameter and β is the scale parameter. While the location parameter determines the position of the function's peak, the scale parameter establishes the width of the peak. The complete specific heat capacity is composed of a linear part and the peak due to the phase transition. The monotonically nondecreasing linear part is motivated by the fact, that the temperature is barely below the Debye-temperature Θ_D and thus has a slightly - almost linear - increasing slope. The total specific heat capacity is fitted with the following function

$$c_p(T) = \left[a_0 + a_1 T + \left(b_0 \cdot \frac{1}{\beta} e^{\frac{T-\mu}{\beta}} \cdot e^{-e^{\frac{T-\mu}{\beta}}} \right) \right] \cdot 1000 \frac{J}{kg \cdot K} \tag{4.5}$$

For the fitting of the specific heat capacity, the following parameters, borrowed from experimental data from the AIT's database were used as initial parameters.

$\boldsymbol{a_0}$	$\boldsymbol{a_1}$	$\boldsymbol{b_0}$	$\boldsymbol{\beta}$	$\boldsymbol{\mu}$
1.9331	0.0152	601.5772	9.3896	126.5000

Table 4.4: Initial parameters for the specific heat capacity function c_p

4.2.3 Fitting Results

To determine the apparent specific heat capacity an iterative procedure was applied. At first a parameter fitting to the experimental data for the function in Eq. 4.5 was carried out. The fitting process was realized with the non-linear least square method for the 5 parameters in the function of the specific heat capacity.

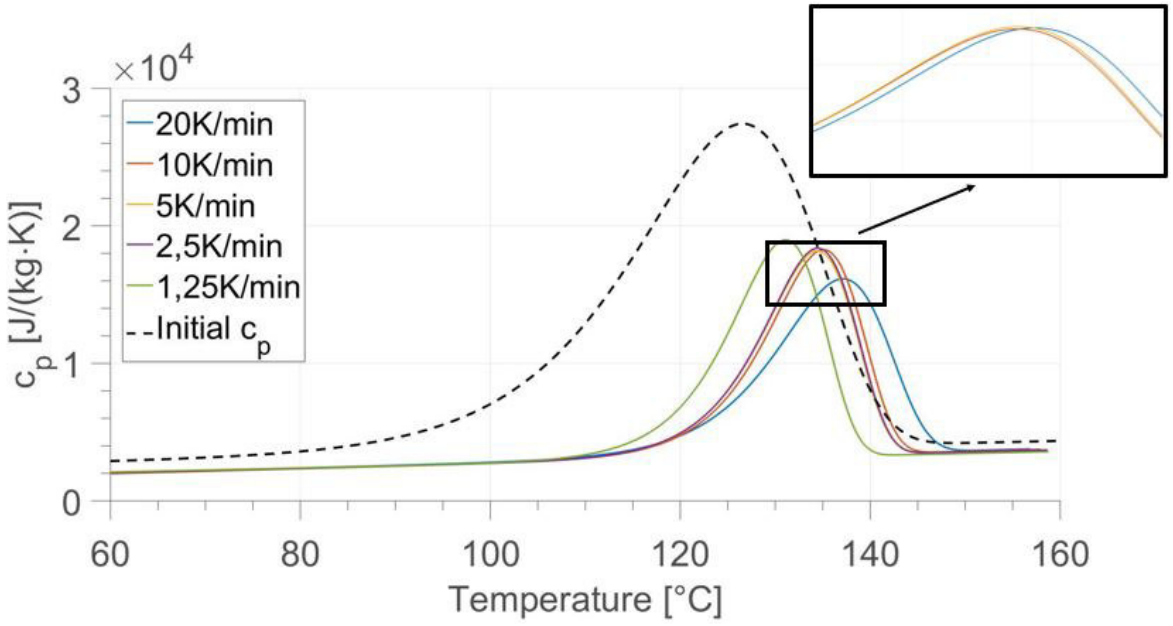

Figure 4.11: Comparison of newly obtained specific heat capacities with the initial specific heat capacity - Black: initial c_p

Now with these parameters a new specific heat curve could be obtained. A comparison between the new curves and the initial curve is illustrated in Fig. 4.11. A simulation with the newly obtained parameters for the specific heat capacity delivers a very good result with only slight deviations from the measured temperature.

However, the fitting yields different parameter sets for different heating rates. While the fitting for the rates $\beta = [10; 5; 2.5]K/min$ are almost identical, the heating rates $\beta = [20; 1.25]K/min$ deviate from the rest. These outliers will be discussed later.

Rate $[K/min]$	$\boldsymbol{a_0}$	$\boldsymbol{a_1}$	$\boldsymbol{b_0}$	$\boldsymbol{\beta}$	$\boldsymbol{\mu}$
20	0,954	0,018	196,61	5,682	137,09
10	0,904	0,018	195,16	4,810	135,06
5	1,011	0,017	192,14	4,753	134,40
2,5	1,011	0,017	195,11	4,761	134,45
1,25	1,193	0,015	204,91	4,765	131,07

Table 4.5: Parameter sets for all heating rates obtained via the fitting procedure

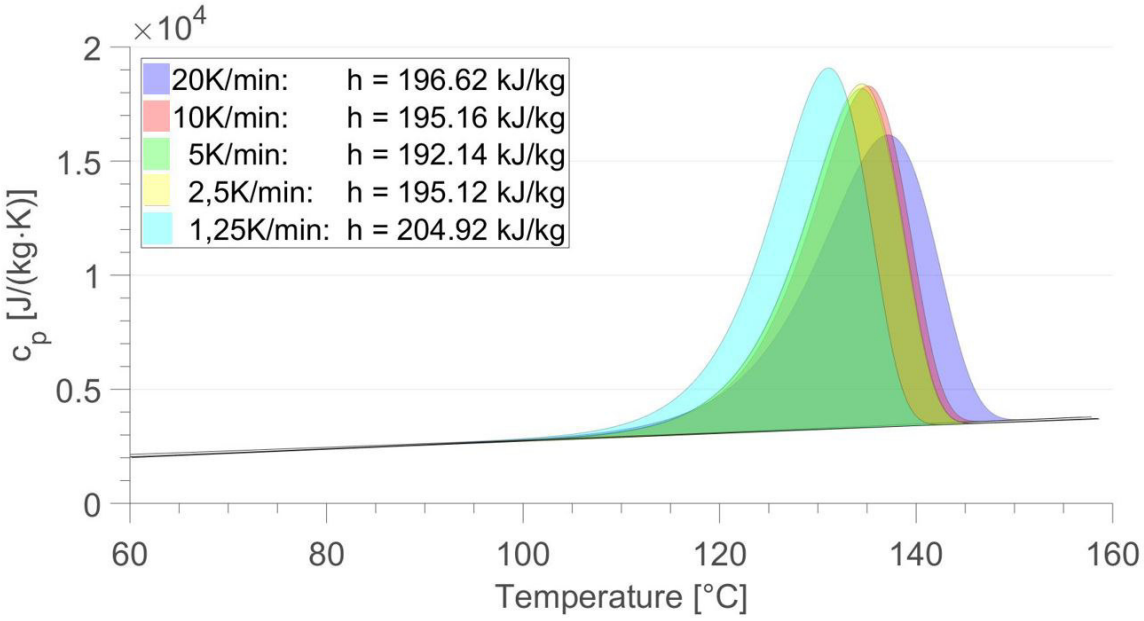

Figure 4.12: Comparison of results of the specific heat capacity simulations for various heating rates

An analysis of the apparent specific heat curves revealed the following parameters: onset temperature (T_{On}), melting temperature (T_{Start}), enthalpy of fusion (h_{melt}), maximum of the specific heat capacity ($c_{p,max}$), the corresponding temperature at which the maximum occurs (T_{max}) and the full width at half maximum (σ).

Rate $[K/min]$	$h_{melt}[kJ/kg]$	T_{Start}	T_{On} $[°C]$
20	196,62	97,5	120,5
10	195,16	102,5	122,1
5	192,14	103,6	121,9
2,5	195,12	103,9	121,8
1,25	204,92	104,7	117,8

Table 4.6: Enthalpy and Onset-Temperature for all heating rates obtained via the fitting procedure

Rate $[K/min]$	$c_{p_{max}}[J/(kgK)]$	T_{max} $[°C]$	σ $[°C]$
20	16150.3	137.2	16.5
10	18298.3	135.0	13.6
5	18179.1	134.4	13.5
2,5	18384.6	134.4	13.6
1,25	19083.2	131.1	13.5

Table 4.7: Curve maximum, reference temperature for the maximum value and the curves full width half maximum for all heating rates obtained via the fitting procedure

Fig. 4.11 and Fig. 4.12 show strong agreement of the curves for the heating rates $\beta = [10; 5; 2.5]K/min$. Table 4.6 shows that for these curves the delay now is almost constant. The coincidence of the specific heat capacity curves implies, that the wide difference of the delay of the melting process in the DSC curves can be explained by different thermal exchange rates, i.e. by the thermal transport kinetics.

The curves for the heating rates $\beta = [20; 1.25]K/min$ exhibit larger deviations. However, these discrepancies can be explained.

The measurement conducted at a heating rate of $\beta = 20K/min$ cannot be regarded for the simulation, because it was the first heating cycle in the DSC process. The sample was originally available in form of beads (diameter: 2-3mm) and therefore it was not compact before the first melting. This means, that the additional air voids between the beads distorted the results, because the thermal conductivity was quite different from that of the following sample after melting.

The deviation for the small heating rate of $\beta = 1.25K/min$ can be explained by the bad signal-to-noise ratio, as it was the case for the sapphire simulation. Additionally, with smaller heating rates it could also be possible that the heat flow through the side and top surface of the crucible, which are not considered in the model, played an increased role.

Summarizing, the simulation of the DSC process with help of the model considering the one dimensional heat conduction, was able to considerably eliminate the rate dependency of the delay's extent of the melting process that can be observed in the DSC measurements. I would point out finally that the remaining delay may be explained by unavoidable for polymer materials discrepancy of the molecular chain length.

Conclusion

The thesis deals with analysis of the melting process in DSC measurements. The DSC technique is a dynamic one, and in order to extract a reliable thermodynamic information for its utilization in design of real thermal storage devices, the influence of particular measurement conditions (sample size, heating rate, etc.) should be investigated. In particular, the delay of the melting process (difference between the starting melting temperature and the onset temperature) and the effect of thermal exchange on it was in the focus of the thesis. For this purpose a model for the DSC process was developed, which was based only on the phenomenon of thermal conduction.

The model with all its assumptions was first tested on a well-known standard in thermophysics, namely sapphire. For most measurement series the simulation was in accordance with the experimental data. For heating rates lower than $\beta = 1,25K/min$, the outcome was not satisfying. The poor results for low heating rates can be traced back to the poor signal-to-noise ratio. Overall, the findings imply the validity of the modelling of the DSC process.

After validating the model, the polyethylene data was subjected to simulation. The parameter fitting with the non-linear least square method was successful in providing a specific heat capacity for the polymer. With this newly obtained thermodynamic property, good results for the simulated temperature of the sample for most heating rates

could be received. As it was in the case of sapphire, heating rates below $\beta = 1,25K/min$ cannot be considered also for the polymer simulation due to the bad signal-to-noise ratio. However, the experimental data obtained with heating rate $\beta = 20K/min$ is also not applicable for analysis because the measurement was distorted due to the initial sample form (the material was available in bead shape, whereas it was compact in all following measurements).

Finally, the simulation, based on the aforementioned model, was able to eliminate the rate dependency of the delay of the melting process. The curves for various heating rates overlapped and thus had the same (intrinsic) melting temperature delay. It is thus not caused by thermal transport kinetics, but rather it is the consequence of the sample's composition. Polymeric systems do not consist of molecular chains of an equal length. There is rather a distribution of the chain length near a most probable value. Being thus not an individual compound, the polymer begins to melt due to "impurities" at a lower temperature than the main substance - thus creating the delay.

While this thesis dealt with the melting process, the solidification is also of great importance for LHTES loading-unloading cycles. Therefore, it would be of high interest to continue the research based on the results of this thesis and expand the understanding to the phase change processes, especially since for the solidification processes a delay due to nucleation must be considered. Furthermore, it could be of interest to analyse in more details the delay in the melting process in dependency of the distribution of the chain length of the polymer.

Bibliography

[1] F. Agyenim, N. Hewitt, P. Eames, and M. Smyth. A review of materials, heat transfer and phase change problem formulation for latent heat thermal energy storage systems (lhtess). Renewable and Sustainable Energy Reviews, 14:615–628, 02 2010.

[2] T. Barz, C. Zauner, D. Lager, D. C. López Cárdenas, F. Hengstberger, M. N. Cruz Bournazou, and K. Marx. Experimental analysis and numerical modeling of a shell and tube heat storage unit with phase change materials. Industrial & Engineering Chemistry Research, 55:8154–8164, 2016.

[3] W. Demtröder. Experimentalphysik 1. Springer, Berlin/Heidelberg, 5., neu bearb. aufl. edition, 2008.

[4] J.-P. Dumas, S. Gibout, L. Zalewski, K. Johannes, E. Franquet, S. Lassue, J.-P. Bédécarrats, P. Tittelein, and F. Kuznik. Interpretation of calorimetry experiments to characterise phase change materials. International Journal of Thermal Sciences, 78:48 – 55, 2014.

[5] V. S. Dusan Medved, Milan Kvakovsky. Latent heat storage systems. PhD thesis, University of West Bohemia, Czech Republic, 2010.

[6] M. M. Farid, A. M. Khudhair, S. A. K. Razack, and S. Al-Hallaj. A review on

phase change energy storage: materials and applications. Energy Conversion and Management, 45(9):1597 – 1615, 2004.

[7] P. Gabbott. A practical introduction to differential scanning calorimetry. 04 2008.

[8] E. Günther, S. Hiebler, H. Mehling, and R. Redlich. Enthalpy of phase change materials as a function of temperature: Required accuracy and suitable measurement methods. International Journal of Thermophysics, 30:1257–1269, 2009.

[9] W. H. G.W.H. Höhne. Differential Scanning Calorimetry. Springer, Berlin/Heidelberg, 2., neu bearb. aufl. edition, 2003.

[10] K. S. H.D. Baehr. Wärme- und Stoffübertragung. Springer, Berlin/Heidelberg, 6., neu bearb. aufl. edition, 2008.

[11] S. Hiebler. Kalorimetrische Methoden zur Bestimmung der Enthalpie von Latentwaermespeichermaterialien waehrend des Phasenuebergangs. PhD thesis, Technische Universitaet Muenchen, 2006.

[12] V. D. Ingenieure. VDI-Wärmeatlas. Springer, Berlin/Heidelberg, 11., neu bearb. aufl. edition, 2013.

[13] X. Jin, X. Xu, X. Zhang, and Y. Yin. Determination of the pcm melting temperature range using dsc. Thermochimica Acta, 595:17 – 21, 2014.

[14] A. M. Khudhair and M. M. Farid. A review on energy conservation in building

applications with thermal storage by latent heat using phase change materials. Energy Conversion and Management, 45(2):263 – 275, 2004.

[15] S. Mondal. 7 - thermo-regulating textiles with phase-change materials. In N. Pan and G. Sun, editors, Functional Textiles for Improved Performance, Protection and Health, Woodhead Publishing Series in Textiles, pages 163 – 183. Woodhead Publishing, 2011.

[16] A. Sharma, V. Tyagi, C. Chen, and D. Buddhi. Review on thermal energy storage with phase change materials and applications. Renewable and Sustainable Energy Reviews, 13(2):318 – 345, 2009.

[17] N. Soares, J. Costa, A. Gaspar, and P. Santos. Review of passive pcm latent heat thermal energy storage systems towards buildings' energy efficiency. Energy and Buildings, 59:82 – 103, 2013.

[18] A. Y. Uzan, Y. Kozak, Y. Korin, I. Harary, H. Mehling, and G. Ziskind. A novel multi-dimensional model for solidification process with supercooling. International Journal of Heat and Mass Transfer, 106:91 – 102, 2017.

[19] B. Zalba, J. M. Marin, L. F. Cabeza, and H. Mehling. Review on thermal energy storage with phase change: materials, heat transfer analysis and applications. Applied Thermal Engineering, 23(3):251 – 283, 2003.

A National Bureau of Standards

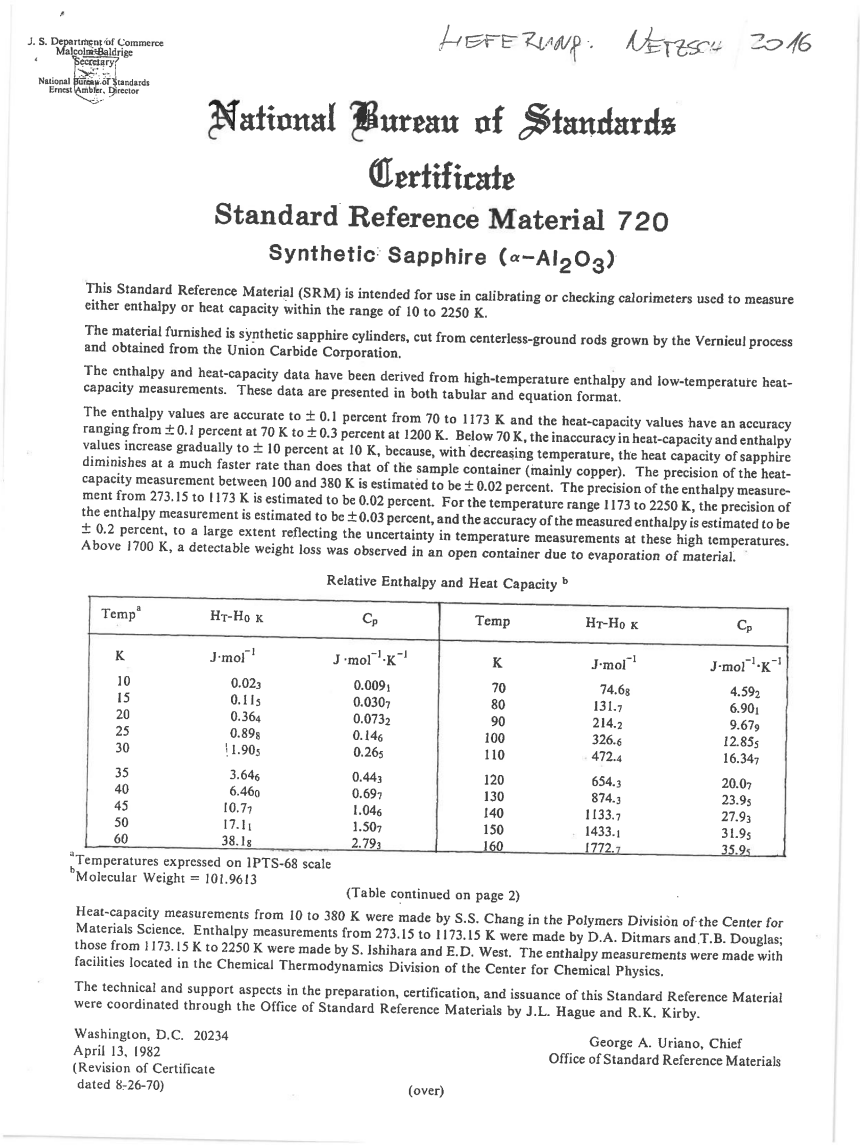

J. S. Department of Commerce
Malcolm Baldrige
Secretary

National Bureau of Standards
Ernest Ambler, Director

LIEFERUNG: NETZSCH 3016

National Bureau of Standards Certificate

Standard Reference Material 720

Synthetic Sapphire (α-Al_2O_3)

This Standard Reference Material (SRM) is intended for use in calibrating or checking calorimeters used to measure either enthalpy or heat capacity within the range of 10 to 2250 K.

The material furnished is synthetic sapphire cylinders, cut from centerless-ground rods grown by the Verneuil process and obtained from the Union Carbide Corporation.

The enthalpy and heat-capacity data have been derived from high-temperature enthalpy and low-temperature heat-capacity measurements. These data are presented in both tabular and equation format.

The enthalpy values are accurate to ± 0.1 percent from 70 to 1173 K and the heat-capacity values have an accuracy ranging from ± 0.1 percent at 70 K to ± 0.3 percent at 1200 K. Below 70 K, the inaccuracy in heat-capacity and enthalpy values increase gradually to ± 10 percent at 10 K, because, with decreasing temperature, the heat capacity of sapphire diminishes at a much faster rate than does that of the sample container (mainly copper). The precision of the heat-capacity measurement between 100 and 380 K is estimated to be ± 0.02 percent. The precision of the enthalpy measurement from 273.15 to 1173 K is estimated to be 0.02 percent. For the temperature range 1173 to 2250 K, the precision of the enthalpy measurement is estimated to be ± 0.03 percent, and the accuracy of the measured enthalpy is estimated to be ± 0.2 percent, to a large extent reflecting the uncertainty in temperature measurements at these high temperatures. Above 1700 K, a detectable weight loss was observed in an open container due to evaporation of material.

Relative Enthalpy and Heat Capacity [b]

Temp[a]	H_T-H_0 K	C_p	Temp	H_T-H_0 K	C_p
K	$J \cdot mol^{-1}$	$J \cdot mol^{-1} \cdot K^{-1}$	K	$J \cdot mol^{-1}$	$J \cdot mol^{-1} \cdot K^{-1}$
10	0.02_3	0.009_1	70	74.6_8	4.59_2
15	0.11_5	0.030_7	80	$131._7$	6.90_1
20	0.36_4	0.073_2	90	$214._2$	9.67_9
25	0.89_8	0.14_6	100	$326._6$	12.85_5
30	1.90_5	0.26_5	110	$472._4$	16.34_7
35	3.64_6	0.44_3	120	$654._3$	20.0_7
40	6.46_0	0.69_7	130	$874._3$	23.9_5
45	10.7_7	1.04_6	140	$1133._7$	27.9_3
50	17.1_1	1.50_7	150	$1433._1$	31.9_5
60	38.1_8	2.79_3	160	$1772._7$	35.9_5

[a] Temperatures expressed on IPTS-68 scale
[b] Molecular Weight = 101.9613

(Table continued on page 2)

Heat-capacity measurements from 10 to 380 K were made by S.S. Chang in the Polymers Division of the Center for Materials Science. Enthalpy measurements from 273.15 to 1173.15 K were made by D.A. Ditmars and T.B. Douglas; those from 1173.15 K to 2250 K were made by S. Ishihara and E.D. West. The enthalpy measurements were made with facilities located in the Chemical Thermodynamics Division of the Center for Chemical Physics.

The technical and support aspects in the preparation, certification, and issuance of this Standard Reference Material were coordinated through the Office of Standard Reference Materials by J.L. Hague and R.K. Kirby.

Washington, D.C. 20234
April 13, 1982
(Revision of Certificate
dated 8-26-70)

George A. Uriano, Chief
Office of Standard Reference Materials

(over)

Relative Enthalpy and Heat Capacity

Temp	H_T-H_0 K	C_p	Temp	H_T-H_0 K	C_p
K	$J \cdot mol^{-1}$	$J \cdot mol^{-1} \cdot K^{-1}$	K	$J \cdot mol^{-1}$	$J \cdot mol^{-1} \cdot K^{-1}$
170	2152.0	39.90	600	40121	112.55
180	2570.3	43.75	610	41249	113.06
190	3026.7	47.50	620	42382	113.55
200	3519.9	51.12	630	43520	114.02
210	4048.7	54.61	640	44663	114.48
220	4611.6	57.95	650	45810	114.92
230	5207.1	61.14	660	46961	115.35
240	5833.9	64.18	670	48117	115.76
250	6490.3	67.08	680	49276	116.16
260	7175.0	69.82	690	50440	116.55
270	7886.3	72.12	700	51607	116.92
273.15	8115.6	73.21	720	53953	117.64
280	8622.8	74.87	740	56313	118.32
290	9383.2	77.20	760	58685	118.96
298.15	10020	79.01	780	61071	119.56
300	10166	79.41	800	63468	120.14
310	10971	81.51	820	65876	120.69
320	11796	83.49	840	68295	121.21
330	12641	85.37	860	70724	121.71
340	13503	87.16	880	73163	122.20
350	14383	88.84	900	75612	122.66
360	15280	90.45	920	78070	123.11
370	16192	91.97	940	80536	123.55
380	17119	93.41	960	83011	123.97
390	18060	94.78	980	85495	124.37
400	19014	96.08	1000	87986	124.77
410	19982	97.32	1020	90486	125.16
420	20961	98.50	1040	92992	125.53
430	21951	99.62	1060	95507	125.90
440	22953	100.69	1080	98028	126.26
450	23965	101.71	1100	100560	126.61
460	24987	102.68	1120	103090	126.95
470	26018	103.60	1140	105640	127.29
480	27059	104.48	1160	108180	127.61
490	28108	105.33	1180	110740	127.94
500	29165	106.13	1200	113300	128.25
510	30230	106.90	1250	119730	129.01
520	31303	107.64	1300	126200	129.74
530	32383	108.35	1350	132710	130.43
540	33470	109.02	1400	139240	131.08
550	34563	109.67	1450	145810	131.70
560	35663	110.29	1500	152410	132.29
570	36769	110.89	1550	159040	132.84
580	37881	111.46	1600	165700	133.36
590	38998	112.02	1650	172380	133.85

Relative Enthalpy and Heat Capacity

Temp	$H_T-H_{0\ K}$	C_p	Temp	$H_T-H_{0\ K}$	C_p
K	$J\cdot mol^{-1}$	$J\cdot mol^{-1}\cdot K^{-1}$	K	$J\cdot mol^{-1}$	$J\cdot mol^{-1}\cdot K^{-1}$
1700	1790_{80}	$134._{31}$	2000	2197_{20}	$136._{50}$
1750	1858_{10}	$134._{73}$	2050	2265_{50}	$136._{80}$
1800	1925_{50}	$135._{13}$	2100	2334_{00}	$137._{10}$
1850	1993_{20}	$135._{50}$	2150	2402_{60}	$137._{41}$
1900	2061_{00}	$135._{85}$	2200	2471_{40}	$137._{73}$
1950	2129_{00}	$136._{18}$	2250	2540_{30}	$138._{06}$

Below 273.15 K, the heat-capacity values were calculated from a spline function fitted to the heat-capacity data over three temperature intervals and employing polynomials, Pn (n = 1,2,3) of the form,

$$Pn = \sum_{i=0}^{6} \frac{A_i}{i!} (T - T_0)^i$$

45.0 K > T ≥ 8.61 K:

$C_p = \exp(P1)\ J\cdot mol^{-1}\cdot K^{-1}$

$T_0 = 8.61$ K

$A_0 = -0.5147E+01$ $A_1 = +0.34127E+00$ $A_2 = -0.333446E-01$ $A_3 = +0.450764E-02$ $A_4 = -0.51464E-03$ $A_5 = +0.397864E-04$ $A_6 = -0.152136E-05$

125.0 K > T ≥ 45.0 K:

$C_p = P2\ J\cdot mol^{-1}\cdot K^{-1}$

$T_0 = 40.0$ K

$A_0 = +0.6966E+00$ $A_1 = +0.59387E-01$ $A_2 = +0.40357E-02$ $A_3 = +0.95173E-04$ $A_4 = -0.35910E-05$ $A_5 = -0.6498E-07$ $A_6 = +0.4089E-08$

273.15 K > T ≥ 125.0 K:

$C_p = P3\ J\cdot mol^{-1}\cdot K^{-1}$

$T_0 = 125.0$ K

$A_0 = +0.21993E+02$ $A_1 = +0.38853E+00$ $A_2 = +0.13955E-02$ $A_3 = -0.83967E-04$ $A_4 = +0.19133E-05$ $A_5 = -0.31778E-07$ $A_6 = +0.29562E-09$

Above 273.15 K, enthalpy and heat-capacity values were derived from the following equation

$$H_T-H_{273.15} = AT^{-2} + BT^{-1} + ClnT + K + DT + ET^2 + FT^3 + GT^4 + HT^5\ J\cdot mol^{-1}$$

A = +6.6253E+07
B = −4.54238E+06
C = −5.475599E+04
K = +2.5819702E+05
D = +2.574076E+02
E = −8.57516E−02
F = +4.299063E−05
G = −1.15192E−08
H = +1.26351E−12

Low-temperature measurements from 10 to 380 K were made with a vacuum adiabatic calorimeter [1,2] operated automatically under the control of a minicomputer. Enthalpy measurements at eighteen temperatures from 273 to 1173 K were made by the drop method using a Bunsen ice calorimeter [3,4]. From 1173 to 2250 K, enthalpy measurements were made with an adiabatic receiving calorimeter [5,6]. All temperatures are expressed on the IPTS-68 scale. In the correction of specimen mass data for atmospheric buoyancy, a density of 3.97 $g\cdot cm^{-3}$ for α-Al_2O_3 was assumed. The functions presented were fitted by the method of least squares to these data. The tabulated values were calculated using these functions.

An occasional particle may contain an end smear due to the method employed in cutting the material. These smears do not contribute significantly to the enthalpy values given in this certificate. However, it is recommended that the material be heated to 1000 °C in air prior to heat-capacity measurements below 350 K. Microprobe analyses indicate small quantities of chloride, titanium, calcium, silicon, iron, copper, and zinc on the surfaces. Spectrographic examination indicates the purity of the bulk material to be at least 99.95 + percent, with the major impurities being magnesium, calcium, chromium, iron, silicon, and titanium. Examination by atomic absorption spectrometry for magnesium, indicated as the major impurity by the above tests, shows that the surface contamination by this element amounts to 1 ppm, or less, and that the bulk material contains 10 ppm, or less, of magnesium. In addition, the material absorbs a small amount (30 ppm or less, presumably moisture) of weight on the ground surfaces on exposure to room air, and may require heating in an inert atmosphere, if this amount of moisture is of concern. Combustion analysis in oxygen indicates the material contains on the order of 10 ppm or less of carbonaceous material calculated as carbon.

B Heat equation - Cartesian coordinates

To set up the heat equation, it is necessary to consider the total energy that enters and exits an infinitesimal segment of matter. Moreover it is essential to look at the energy that could be generated during a transition. Therefore the following energy balance is obtained

$$E_{total} = E_{in} - E_{out} \tag{1}$$

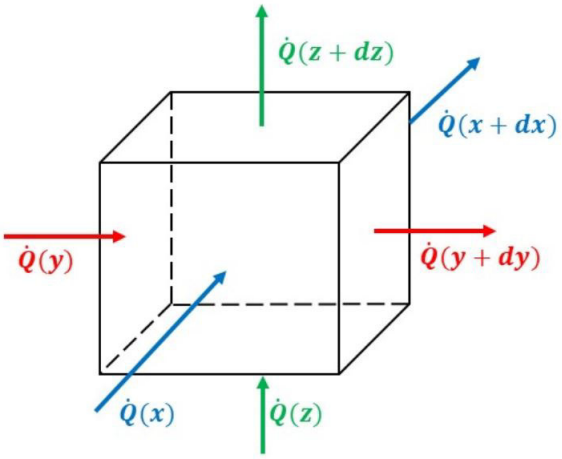

Figure 1: Energy balance for Cartesian coordinates

The individual contributions are as follows

$$E_{total} = mc_p \frac{dT}{dt} \tag{2}$$

$$E_{in} = \dot{Q}_x + \dot{Q}_y + \dot{Q}_z \tag{3}$$

$$E_{out} = \dot{Q}_{x+dx} + \dot{Q}_{y+dy} + \dot{Q}_{z+dz} \tag{4}$$

The heat fluxes that exit the volume are submitted to a Taylor expansion

$$\dot{Q}_{x+dx} = \dot{Q}_x + \frac{\partial \dot{Q}_x}{\partial x} dx \tag{5}$$

$$\dot{Q}_{y+dy} = \dot{Q}_y + \frac{\partial \dot{Q}_y}{\partial y} dy \tag{6}$$

$$\dot{Q}_{z+dz} = \dot{Q}_z + \frac{\partial \dot{Q}_z}{\partial z} dz \tag{7}$$

If the relations above are put into the energy balance equation (1) one obtains

$$\rho c_p \frac{dT}{dt} dxdydz = -\frac{\partial \dot{Q}_x}{\partial x} dx - \frac{\partial \dot{Q}_y}{\partial y} dy - \frac{\partial \dot{Q}_z}{\partial z} dz \tag{8}$$

With Fouriers law (2.4) the infinitesimal volume $dV = dxdydz$ cancels out and the final form is then received

$$\begin{aligned}\rho c_p \frac{dT}{dt} dxdydz = &- \frac{\partial}{\partial x}\left(-\lambda dydz \cdot \frac{\partial T}{\partial x}\right) dx \\ &- \frac{\partial}{\partial y}\left(-\lambda dxdz \cdot \frac{\partial T}{\partial y}\right) dy \\ &- \frac{\partial}{\partial z}\left(-\lambda dxdy \cdot \frac{\partial T}{\partial z}\right) dz\end{aligned} \tag{9}$$

$$\boxed{\rho c_p \frac{dT}{dt} = \frac{\partial}{\partial x}\left(\lambda \frac{\partial T}{\partial x}\right) + \frac{\partial}{\partial y}\left(\lambda \frac{\partial T}{\partial y}\right) + \frac{\partial}{\partial z}\left(\lambda \frac{\partial T}{\partial z}\right)} \tag{10}$$

C Heat equation - Cylindrical coordinates

In this section the process of deriving the heat equation for a cylinder is going to be shown. At first an infinitesimal cylindrical volume is considered and then the energy balance is set up (1). The sample assumes a cylindrical shape.

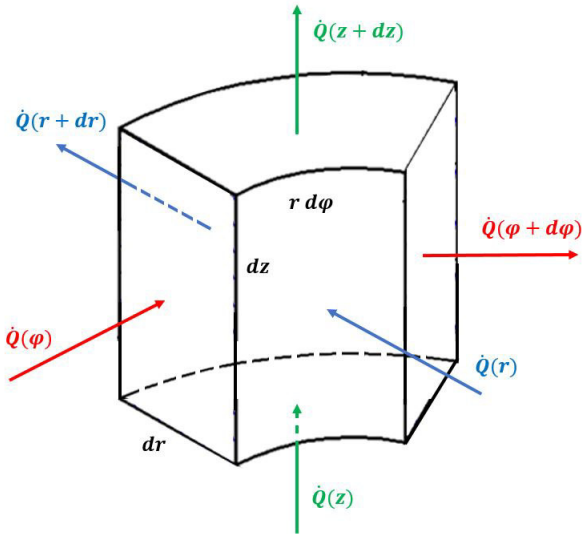

Figure 2: Energy balance for cylindrical coordinates

The individual contributions are as follows

$$E_{total} = mc_p \frac{dT}{dt} \tag{11}$$

$$E_{in} = \dot{Q}_r + \dot{Q}_\varphi + \dot{Q}_z \tag{12}$$

$$E_{out} = \dot{Q}_{r+dr} + \dot{Q}_{\varphi+d\varphi} + \dot{Q}_{z+dz} \tag{13}$$

The Taylor expansion yields the terms

$$\dot{Q}_{r+dr} = \dot{Q}_r + \frac{\partial \dot{Q}_r}{\partial r} dr \tag{14}$$

$$\dot{Q}_{\varphi+d\varphi} = \dot{Q}_\varphi + \frac{\partial \dot{Q}_\varphi}{\partial \varphi} d\varphi \tag{15}$$

$$\dot{Q}_{z+dz} = \dot{Q}_z + \frac{\partial \dot{Q}_z}{\partial z} dz \tag{16}$$

Furthermore Fourier's low provides the following relations

$$\frac{\partial \dot{Q}_r}{\partial r} dr = -\frac{\partial}{\partial r}\left(\lambda \cdot r d\varphi \cdot dz \cdot \frac{\partial T}{\partial r}\right) dr \tag{17}$$

$$\frac{\partial \dot{Q}_\varphi}{\partial \varphi} d\varphi = -\frac{\partial}{\partial \varphi}\left(\lambda \cdot dr \cdot dz \cdot \frac{1}{r} \cdot \frac{\partial T}{\partial \varphi}\right) d\varphi \tag{18}$$

$$\frac{\partial \dot{Q}_z}{\partial z} dz = -\frac{\partial}{\partial z}\left(\lambda \cdot r d\varphi \cdot dr \cdot \frac{\partial T}{\partial z}\right) dz \tag{19}$$

$$\boxed{\rho c_p \frac{\partial T}{\partial t} = \frac{1}{r}\frac{\partial}{\partial r}\left(\lambda \cdot r \frac{\partial T}{\partial r}\right) + \frac{1}{r^2}\frac{\partial}{\partial \varphi}\left(\lambda \frac{\partial T}{\partial \varphi}\right) + \frac{\partial}{\partial z}\left(\lambda \frac{\partial T}{\partial z}\right)} \tag{20}$$

With the Laplace operator this can also be written in the following form

$$\boxed{\rho c_p \frac{\partial T}{\partial t} = \nabla(\lambda \vec{\nabla} T)} \tag{21}$$

As described in [4] it can also be written in the following enthalpic form

$$\boxed{\frac{\partial \rho h}{\partial t} = \nabla \cdot (\lambda \vec{\nabla} T)} \tag{22}$$

D Electrochemical series of type E thermocouple

Thermoelement-Referenztabellen

TYP E

Referenztabellen N.I.S.T. Monograph 175 Nach ITS-90

Nickel-Chrom und Kupfer-Nickel

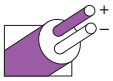

IEC-584-3 Farbcodierung: Thermoelement- und Ausgleichs-leitung

MAXIMALER TEMPERATURBEREICH
Thermoelementleitung
–328 bis 1652°F, –200 bis 900°C
Verlängerungsleitung
32 bis 392°F, 0 bis 200°C
FEHLERTOLERANZEN
(je nachdem, welcher Wert größer ist)
Standard: 1,7°C oder 0,5% über 0°C, 1,7°C oder 1,0% unter 0°C
Besonders enge Fehlertoleranz: 1,0°C oder 0,4%
KOMMENTARE, UMGEBUNG FÜR UNISOLIERTE LEITUNGEN:
Oxidierend oder chemisch inaktiv; Nur begrenzt einsetzbar in Vakuum oder reduzierender Umgebung; Größte Änderung der EMK pro Grad
TEMPERATUR IN °C
VERGLEICHSSTELLE BEI 0°C

Thermoelektrische Spannung in mV

°C	-10	-9	-8	-7	-6	-5	-4	-3	-2	-1	0	°C
-260	-9.835	-9.833	-9.831	-9.828	-9.825	-9.821	-9.817	-9.813	-9.808	-9.802	-9.797	-260
-250	-9.797	-9.790	-9.784	-9.777	-9.770	-9.762	-9.754	-9.746	-9.737	-9.728	-9.718	-250
-240	-9.718	-9.709	-9.698	-9.688	-9.677	-9.666	-9.654	-9.642	-9.630	-9.617	-9.604	-240
-230	-9.604	-9.591	-9.577	-9.563	-9.548	-9.534	-9.519	-9.503	-9.487	-9.471	-9.455	-230
-220	-9.455	-9.438	-9.421	-9.404	-9.386	-9.368	-9.350	-9.331	-9.313	-9.293	-9.274	-220
-210	-9.274	-9.254	-9.234	-9.214	-9.193	-9.172	-9.151	-9.129	-9.107	-9.085	-9.063	-210
-200	-9.063	-9.040	-9.017	-8.994	-8.971	-8.947	-8.923	-8.899	-8.874	-8.850	-8.825	-200
-190	-8.825	-8.799	-8.774	-8.748	-8.722	-8.696	-8.669	-8.643	-8.616	-8.588	-8.561	-190
-180	-8.561	-8.533	-8.505	-8.477	-8.449	-8.420	-8.391	-8.362	-8.333	-8.303	-8.273	-180
-170	-8.273	-8.243	-8.213	-8.183	-8.152	-8.121	-8.090	-8.059	-8.027	-7.995	-7.963	-170
-160	-7.963	-7.931	-7.899	-7.866	-7.833	-7.800	-7.767	-7.733	-7.700	-7.666	-7.632	-160
-150	-7.632	-7.597	-7.563	-7.528	-7.493	-7.458	-7.423	-7.387	-7.351	-7.315	-7.279	-150
-140	-7.279	-7.243	-7.206	-7.170	-7.133	-7.096	-7.058	-7.021	-6.983	-6.945	-6.907	-140
-130	-6.907	-6.869	-6.831	-6.792	-6.753	-6.714	-6.675	-6.636	-6.596	-6.556	-6.516	-130
-120	-6.516	-6.476	-6.436	-6.396	-6.355	-6.314	-6.273	-6.232	-6.191	-6.149	-6.107	-120
-110	-6.107	-6.065	-6.023	-5.981	-5.939	-5.896	-5.853	-5.810	-5.767	-5.724	-5.681	-110
-100	-5.681	-5.637	-5.593	-5.549	-5.505	-5.461	-5.417	-5.372	-5.327	-5.282	-5.237	-100
-90	-5.237	-5.192	-5.147	-5.101	-5.055	-5.009	-4.963	-4.917	-4.871	-4.824	-4.777	-90
-80	-4.777	-4.731	-4.684	-4.636	-4.589	-4.542	-4.494	-4.446	-4.398	-4.350	-4.302	-80
-70	-4.302	-4.254	-4.205	-4.156	-4.107	-4.058	-4.009	-3.960	-3.911	-3.861	-3.811	-70
-60	-3.811	-3.761	-3.711	-3.661	-3.611	-3.561	-3.510	-3.459	-3.408	-3.357	-3.306	-60
-50	-3.306	-3.255	-3.204	-3.152	-3.100	-3.048	-2.996	-2.944	-2.892	-2.840	-2.787	-50
-40	-2.787	-2.735	-2.682	-2.629	-2.576	-2.523	-2.469	-2.416	-2.362	-2.309	-2.255	-40
-30	-2.255	-2.201	-2.147	-2.093	-2.038	-1.984	-1.929	-1.874	-1.820	-1.765	-1.709	-30
-20	-1.709	-1.654	-1.599	-1.543	-1.488	-1.432	-1.376	-1.320	-1.264	-1.208	-1.152	-20
-10	-1.152	-1.095	-1.039	-0.982	-0.925	-0.868	-0.811	-0.754	-0.697	-0.639	-0.582	-10
0	-0.582	-0.524	-0.466	-0.408	-0.350	-0.292	-0.234	-0.176	-0.117	-0.059	0.000	0
0	0.000	0.059	0.118	0.176	0.235	0.294	0.354	0.413	0.472	0.532	0.591	0
10	0.591	0.651	0.711	0.770	0.830	0.890	0.950	1.010	1.071	1.131	1.192	10
20	1.192	1.252	1.313	1.373	1.434	1.495	1.556	1.617	1.678	1.740	1.801	20
30	1.801	1.862	1.924	1.986	2.047	2.109	2.171	2.233	2.295	2.357	2.420	30
40	2.420	2.482	2.545	2.607	2.670	2.733	2.795	2.858	2.921	2.984	3.048	40
50	3.048	3.111	3.174	3.238	3.301	3.365	3.429	3.492	3.556	3.620	3.685	50
60	3.685	3.749	3.813	3.877	3.942	4.006	4.071	4.136	4.200	4.265	4.330	60
70	4.330	4.395	4.460	4.526	4.591	4.656	4.722	4.788	4.853	4.919	4.985	70
80	4.985	5.051	5.117	5.183	5.249	5.315	5.382	5.448	5.514	5.581	5.648	80
90	5.648	5.714	5.781	5.848	5.915	5.982	6.049	6.117	6.184	6.251	6.319	90
100	6.319	6.386	6.454	6.522	6.590	6.658	6.725	6.794	6.862	6.930	6.998	100
110	6.998	7.066	7.135	7.203	7.272	7.341	7.409	7.478	7.547	7.616	7.685	110
120	7.685	7.754	7.823	7.892	7.962	8.031	8.101	8.170	8.240	8.309	8.379	120
130	8.379	8.449	8.519	8.589	8.659	8.729	8.799	8.869	8.940	9.010	9.081	130
140	9.081	9.151	9.222	9.292	9.363	9.434	9.505	9.576	9.647	9.718	9.789	140
150	9.789	9.860	9.931	10.003	10.074	10.145	10.217	10.288	10.360	10.432	10.503	150
160	10.503	10.575	10.647	10.719	10.791	10.863	10.935	11.007	11.080	11.152	11.224	160
170	11.224	11.297	11.369	11.442	11.514	11.587	11.660	11.733	11.805	11.878	11.951	170
180	11.951	12.024	12.097	12.170	12.243	12.317	12.390	12.463	12.537	12.610	12.684	180
190	12.684	12.757	12.831	12.904	12.978	13.052	13.126	13.199	13.273	13.347	13.421	190
200	13.421	13.495	13.569	13.644	13.718	13.792	13.866	13.941	14.015	14.090	14.164	200
210	14.164	14.239	14.313	14.388	14.463	14.537	14.612	14.687	14.762	14.837	14.912	210
220	14.912	14.987	15.062	15.137	15.212	15.287	15.362	15.438	15.513	15.588	15.664	220
230	15.664	15.739	15.815	15.890	15.966	16.041	16.117	16.193	16.269	16.344	16.420	230
240	16.420	16.496	16.572	16.648	16.724	16.800	16.876	16.952	17.028	17.104	17.181	240
250	17.181	17.257	17.333	17.409	17.486	17.562	17.639	17.715	17.792	17.868	17.945	250
260	17.945	18.021	18.098	18.175	18.252	18.328	18.405	18.482	18.559	18.636	18.713	260
270	18.713	18.790	18.867	18.944	19.021	19.098	19.175	19.252	19.330	19.407	19.484	270
280	19.484	19.561	19.639	19.716	19.794	19.871	19.948	20.026	20.103	20.181	20.259	280
290	20.259	20.336	20.414	20.492	20.569	20.647	20.725	20.803	20.880	20.958	21.036	290
300	21.036	21.114	21.192	21.270	21.348	21.426	21.504	21.582	21.660	21.739	21.817	300
310	21.817	21.895	21.973	22.051	22.130	22.208	22.286	22.365	22.443	22.522	22.600	310
320	22.600	22.678	22.757	22.835	22.914	22.993	23.071	23.150	23.228	23.307	23.386	320
330	23.386	23.464	23.543	23.622	23.701	23.780	23.858	23.937	24.016	24.095	24.174	330
340	24.174	24.253	24.332	24.411	24.490	24.569	24.648	24.727	24.806	24.885	24.964	340
°C	0	1	2	3	4	5	6	7	8	9	10	°C

°C	0	1	2	3	4	5	6	7	8	9	10	°C
350	24.964	25.044	25.123	25.202	25.281	25.360	25.440	25.519	25.598	25.678	25.757	350
360	25.757	25.836	25.916	25.995	26.075	26.154	26.233	26.313	26.392	26.472	26.552	360
370	26.552	26.631	26.711	26.790	26.870	26.950	27.029	27.109	27.189	27.268	27.348	370
380	27.348	27.428	27.507	27.587	27.667	27.747	27.827	27.907	27.986	28.066	28.146	380
390	28.146	28.226	28.306	28.386	28.466	28.546	28.626	28.706	28.786	28.866	28.946	390
400	28.946	29.026	29.106	29.186	29.266	29.346	29.427	29.507	29.587	29.667	29.747	400
410	29.747	29.827	29.908	29.988	30.068	30.148	30.229	30.309	30.389	30.470	30.550	410
420	30.550	30.630	30.711	30.791	30.871	30.952	31.032	31.112	31.193	31.273	31.354	420
430	31.354	31.434	31.515	31.595	31.676	31.756	31.837	31.917	31.998	32.078	32.159	430
440	32.159	32.239	32.320	32.400	32.481	32.562	32.642	32.723	32.803	32.884	32.965	440
450	32.965	33.045	33.126	33.207	33.287	33.368	33.449	33.529	33.610	33.691	33.772	450
460	33.772	33.852	33.933	34.014	34.095	34.175	34.256	34.337	34.418	34.498	34.579	460
470	34.579	34.660	34.741	34.822	34.902	34.983	35.064	35.145	35.226	35.307	35.387	470
480	35.387	35.468	35.549	35.630	35.711	35.792	35.873	35.954	36.034	36.115	36.196	480
490	36.196	36.277	36.358	36.439	36.520	36.601	36.682	36.763	36.843	36.924	37.005	490
500	37.005	37.086	37.167	37.248	37.329	37.410	37.491	37.572	37.653	37.734	37.815	500
510	37.815	37.896	37.977	38.058	38.139	38.220	38.300	38.381	38.462	38.543	38.624	510
520	38.624	38.705	38.786	38.867	38.948	39.029	39.110	39.191	39.272	39.353	39.434	520
530	39.434	39.515	39.596	39.677	39.758	39.839	39.920	40.001	40.082	40.163	40.243	530
540	40.243	40.324	40.405	40.486	40.567	40.648	40.729	40.810	40.891	40.972	41.053	540
550	41.053	41.134	41.215	41.296	41.377	41.457	41.538	41.619	41.700	41.781	41.862	550
560	41.862	41.943	42.024	42.105	42.185	42.266	42.347	42.428	42.509	42.590	42.671	560
570	42.671	42.751	42.832	42.913	42.994	43.075	43.156	43.236	43.317	43.398	43.479	570
580	43.479	43.560	43.640	43.721	43.802	43.883	43.963	44.044	44.125	44.206	44.286	580
590	44.286	44.367	44.448	44.529	44.609	44.690	44.771	44.851	44.932	45.013	45.093	590
600	45.093	45.174	45.255	45.335	45.416	45.497	45.577	45.658	45.738	45.819	45.900	600
610	45.900	45.980	46.061	46.141	46.222	46.302	46.383	46.463	46.544	46.624	46.705	610
620	46.705	46.785	46.866	46.946	47.027	47.107	47.188	47.268	47.349	47.429	47.509	620
630	47.509	47.590	47.670	47.751	47.831	47.911	47.992	48.072	48.152	48.233	48.313	630
640	48.313	48.393	48.474	48.554	48.634	48.715	48.795	48.875	48.955	49.035	49.116	640
650	49.116	49.196	49.276	49.356	49.436	49.517	49.597	49.677	49.757	49.837	49.917	650
660	49.917	49.997	50.077	50.157	50.238	50.318	50.398	50.478	50.558	50.638	50.718	660
670	50.718	50.798	50.878	50.958	51.038	51.118	51.197	51.277	51.357	51.437	51.517	670
680	51.517	51.597	51.677	51.757	51.837	51.916	51.996	52.076	52.156	52.236	52.315	680
690	52.315	52.395	52.475	52.555	52.634	52.714	52.794	52.873	52.953	53.033	53.112	690
700	53.112	53.192	53.272	53.351	53.431	53.510	53.590	53.670	53.749	53.829	53.908	700
710	53.908	53.988	54.067	54.147	54.226	54.306	54.385	54.465	54.544	54.624	54.703	710
720	54.703	54.782	54.862	54.941	55.021	55.100	55.179	55.259	55.338	55.417	55.497	720
730	55.497	55.576	55.655	55.734	55.814	55.893	55.972	56.051	56.131	56.210	56.289	730
740	56.289	56.368	56.447	56.526	56.606	56.685	56.764	56.843	56.922	57.001	57.080	740
750	57.080	57.159	57.238	57.317	57.396	57.475	57.554	57.633	57.712	57.791	57.870	750
760	57.870	57.949	58.028	58.107	58.186	58.265	58.343	58.422	58.501	58.580	58.659	760
770	58.659	58.738	58.816	58.895	58.974	59.053	59.131	59.210	59.289	59.367	59.446	770
780	59.446	59.525	59.604	59.682	59.761	59.839	59.918	59.997	60.075	60.154	60.232	780
790	60.232	60.311	60.390	60.468	60.547	60.625	60.704	60.782	60.860	60.939	61.017	790
800	61.017	61.096	61.174	61.253	61.331	61.409	61.488	61.566	61.644	61.723	61.801	800
810	61.801	61.879	61.958	62.036	62.114	62.192	62.271	62.349	62.427	62.505	62.583	810
820	62.583	62.662	62.740	62.818	62.896	62.974	63.052	63.130	63.208	63.286	63.364	820
830	63.364	63.442	63.520	63.598	63.676	63.754	63.832	63.910	63.988	64.066	64.144	830
840	64.144	64.222	64.300	64.377	64.455	64.533	64.611	64.689	64.766	64.844	64.922	840
850	64.922	65.000	65.077	65.155	65.233	65.310	65.388	65.465	65.543	65.621	65.698	850
860	65.698	65.776	65.853	65.931	66.008	66.086	66.163	66.241	66.318	66.396	66.473	860
870	66.473	66.550	66.628	66.705	66.782	66.860	66.937	67.014	67.092	67.169	67.246	870
880	67.246	67.323	67.400	67.478	67.555	67.632	67.709	67.786	67.863	67.940	68.017	880
890	68.017	68.094	68.171	68.248	68.325	68.402	68.479	68.556	68.633	68.710	68.787	890
900	68.787	68.863	68.940	69.017	69.094	69.171	69.247	69.324	69.401	69.477	69.554	900
910	69.554	69.631	69.707	69.784	69.860	69.937	70.013	70.090	70.166	70.243	70.319	910
920	70.319	70.396	70.472	70.548	70.625	70.701	70.777	70.854	70.930	71.006	71.082	920
930	71.082	71.159	71.235	71.311	71.387	71.463	71.539	71.615	71.692	71.768	71.844	930
940	71.844	71.920	71.996	72.072	72.147	72.223	72.299	72.375	72.451	72.527	72.603	940
950	72.603	72.678	72.754	72.830	72.906	72.981	73.057	73.133	73.208	73.284	73.360	950
960	73.360	73.435	73.511	73.586	73.662	73.738	73.813	73.889	73.964	74.040	74.115	960
970	74.115	74.190	74.266	74.341	74.417	74.492	74.567	74.643	74.718	74.793	74.869	970
980	74.869	74.944	75.019	75.095	75.170	75.245	75.320	75.395	75.471	75.546	75.621	980
990	75.621	75.696	75.771	75.847	75.922	75.997	76.072	76.147	76.223	76.298	76.373	990
°C	0	1	2	3	4	5	6	7	8	9	10	°C

E DIN EN ISO 11357-4

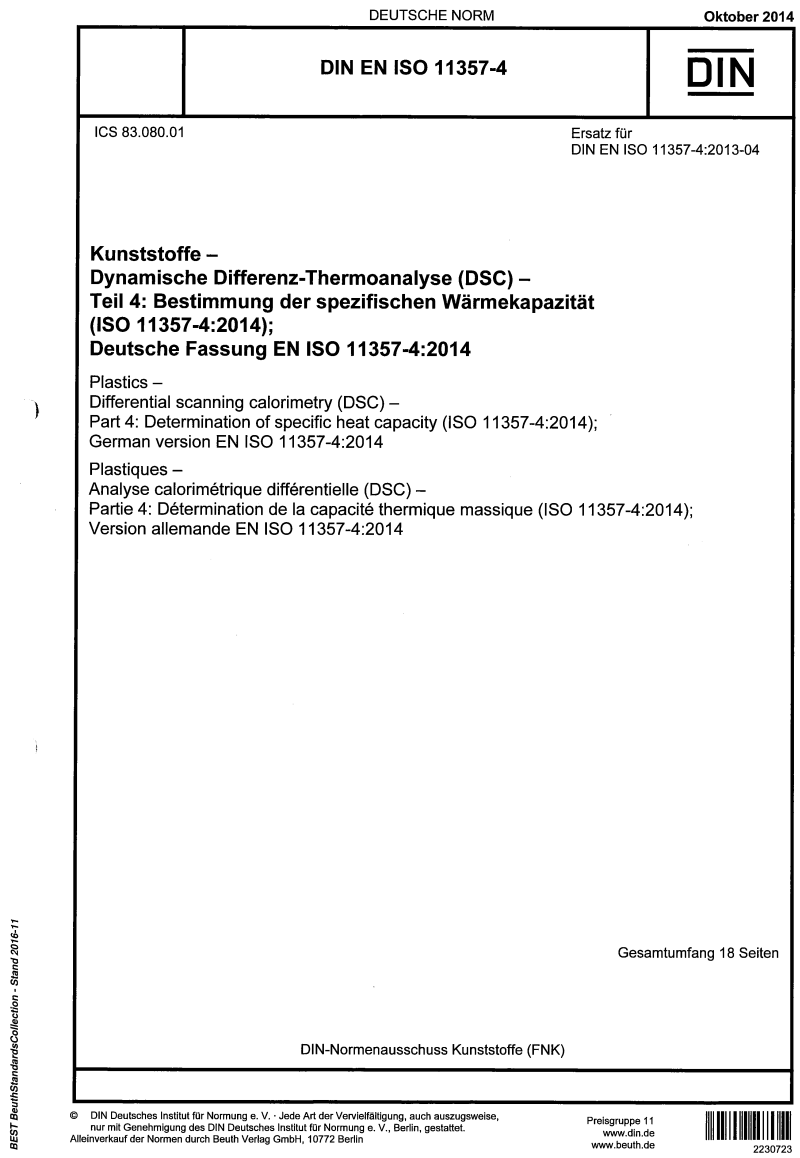

DEUTSCHE NORM **Oktober 2014**

DIN EN ISO 11357-4

DIN

ICS 83.080.01

Ersatz für
DIN EN ISO 11357-4:2013-04

Kunststoffe –
Dynamische Differenz-Thermoanalyse (DSC) –
Teil 4: Bestimmung der spezifischen Wärmekapazität
(ISO 11357-4:2014);
Deutsche Fassung EN ISO 11357-4:2014

Plastics –
Differential scanning calorimetry (DSC) –
Part 4: Determination of specific heat capacity (ISO 11357-4:2014);
German version EN ISO 11357-4:2014

Plastiques –
Analyse calorimétrique différentielle (DSC) –
Partie 4: Détermination de la capacité thermique massique (ISO 11357-4:2014);
Version allemande EN ISO 11357-4:2014

Gesamtumfang 18 Seiten

DIN-Normenausschuss Kunststoffe (FNK)

Preisgruppe 11
www.din.de
www.beuth.de
2230723

Nationales Vorwort

Dieses Dokument (EN ISO 11357-4:2014) wurde vom Technischen Komitee ISO/TC 61 „Plastics" in Zusammenarbeit mit dem Technischen Komitee CEN/TC 249 „Kunststoffe" erarbeitet, dessen Sekretariat vom NBN (Belgien) gehalten wird.

Das zuständige nationale Normungsgremium ist der Arbeitsausschuss NA 054-01-03 AA „Physikalische, rheologische und analytische Prüfungen" im DIN-Normenausschuss „Kunststoffe" (FNK).

DIN EN ISO 11357 mit dem allgemeinen Titel *Kunststoffe — Dynamische Differenz-Thermoanalyse (DSC)* besteht aus den folgenden Teilen:

— *Teil 1: Allgemeine Grundlagen*

— *Teil 2: Bestimmung der Glasübergangstemperatur und der Glasübergangsstufen*

— *Teil 3: Bestimmung der Schmelz- und Kristallisationstemperatur und der Schmelz- und Kristallisationsenthalpie*

— *Teil 4: Bestimmung der spezifischen Wärmekapazität*

— *Teil 5: Bestimmung von charakteristischen Reaktionstemperaturen und -zeiten, Reaktionsenthalpie und Umsatz*

— *Teil 6: Bestimmung der Oxidations-Induktions-Zeit (isothermische IOT) und Oxidations-Induktions-Temperatur (dynamische OIT)*

— *Teil 7: Bestimmung der Kristallisationskinetik*

Für die in diesem Dokument zitierten Normen wird im Folgenden auf die entsprechenden Deutschen Normen hingewiesen:

ISO 472	siehe	DIN EN ISO 472
ISO 11357-1	siehe	DIN EN ISO 11357-1

Änderungen

Gegenüber DIN EN ISO 11357-4:2013-04 wurden folgende Änderungen vorgenommen:

a) alle normativen Verweisungen wurden in undatierte geändert;

b) in der englischen Fassung wurde der Begriff „pan" im ganzen Dokument durch „crucible" ersetzt. In der deutschen Fassung bleibt der Begriff „Tiegel" bestehen;

c) die endotherme Richtung „a" wurde in allen Bildern und Legenden ergänzt.

Frühere Ausgaben

DIN EN ISO 11357-4: 2013-04

Nationaler Anhang NA
(informativ)

Literaturhinweise

DIN EN ISO 472, *Kunststoffe — Fachwörterverzeichnis*

DIN EN ISO 11357-1, *Kunststoffe — Dynamische Differenz-Thermoanalyse (DSC) — Teil 1: Allgemeine Grundlagen*

— Leerseite —

EUROPÄISCHE NORM

EUROPEAN STANDARD

NORME EUROPÉENNE

EN ISO 11357-4

Juni 2014

ICS 83.080.01

Ersatz für EN ISO 11357-4:2013

Deutsche Fassung

Kunststoffe — Dynamische Differenz-Thermoanalyse (DSC) — Teil 4: Bestimmung der spezifischen Wärmekapazität (ISO 11357-4:2014)

Plastics — Differential scanning calorimetry (DSC) — Part 4: Determination of specific heat capacity (ISO 11357-4:2014)

Plastiques — Analyse calorimétrique différentielle (DSC) — Partie 4: Détermination de la capacité thermique massique (ISO 11357-4:2014)

Diese Europäische Norm wurde vom CEN am 10. Juli 2014 angenommen.

Die CEN-Mitglieder sind gehalten, die CEN/CENELEC-Geschäftsordnung zu erfüllen, in der die Bedingungen festgelegt sind, unter denen dieser Europäischen Norm ohne jede Änderung der Status einer nationalen Norm zu geben ist. Auf dem letzten Stand befindliche Listen dieser nationalen Normen mit ihren bibliographischen Angaben sind beim Management-Zentrum des CEN-CENELEC oder bei jedem CEN-Mitglied auf Anfrage erhältlich.

Diese Europäische Norm besteht in drei offiziellen Fassungen (Deutsch, Englisch, Französisch). Eine Fassung in einer anderen Sprache, die von einem CEN-Mitglied in eigener Verantwortung durch Übersetzung in seine Landessprache gemacht und dem Management-Zentrum mitgeteilt worden ist, hat den gleichen Status wie die offiziellen Fassungen.

CEN-Mitglieder sind die nationalen Normungsinstitute von Belgien, Bulgarien, Dänemark, Deutschland, der ehemaligen jugoslawischen Republik Mazedonien, Estland, Finnland, Frankreich, Griechenland, Irland, Island, Italien, Kroatien, Lettland, Litauen, Luxemburg, Malta, den Niederlanden, Norwegen, Österreich, Polen, Portugal, Rumänien, Schweden, der Schweiz, der Slowakei, Slowenien, Spanien, der Tschechischen Republik, der Türkei, Ungarn, dem Vereinigten Königreich und Zypern.

EUROPÄISCHES KOMITEE FÜR NORMUNG
EUROPEAN COMMITTEE FOR STANDARDIZATION
COMITÉ EUROPÉEN DE NORMALISATION

CEN-CENELEC Management-Zentrum: Avenue Marnix 17, B-1000 Brüssel

Ref. Nr. EN ISO 11357-4:2014 D

Inhalt

Vorwort

Dieses Dokument (EN ISO 11357-4:2014) wurde vom Technischen Komitee ISO/TC 61 „Plastics" in Zusammenarbeit mit dem Technischen Komitee CEN/TC 249 „Kunststoffe" erarbeitet, dessen Sekretariat vom NBN gehalten wird.

Diese Europäische Norm muss den Status einer nationalen Norm erhalten, entweder durch Veröffentlichung eines identischen Textes oder durch Anerkennung bis Dezember 2014, und etwaige entgegenstehende nationale Normen müssen bis Dezember 2014 zurückgezogen werden.

Es wird auf die Möglichkeit hingewiesen, dass einige Elemente dieses Dokuments Patentrechte berühren können. CEN [und/oder CENELEC] sind nicht dafür verantwortlich, einige oder alle diesbezüglichen Patentrechte zu identifizieren.

Dieses Dokument ersetzt EN ISO 11357-4:2013.

Gegenüber EN ISO 11357-4:2013 wurden folgende Änderungen vorgenommen:

a) alle normativen Verweisungen wurden in undatierte geändert;

b) in der englischen Fassung wurde der Begriff „pan" im ganzen Dokument durch „crucible" ersetzt. In der deutschen Fassung bleibt der Begriff „Tiegel" bestehen;

c) die endotherme Richtung „a" wurde in allen Bildern und Legenden ergänzt.

EN ISO 11357 mit dem allgemeinen Titel *Kunststoffe — Dynamische Differenz-Thermoanalyse (DSC)* besteht aus den folgenden Teilen:

— *Teil 1: Allgemeine Grundlagen*

— *Teil 2: Bestimmung der Glasübergangstemperatur und der Glasübergangsstufen*

— *Teil 3: Bestimmung der Schmelz- und Kristallisationstemperatur und der Schmelz- und Kristallisationsenthalpie*

— *Teil 4: Bestimmung der spezifischen Wärmekapazität*

— *Teil 5: Bestimmung von charakteristischen Reaktionstemperaturen und -zeiten, Reaktionsenthalpie und Umsatz*

— *Teil 6: Bestimmung der Oxidations-Induktions-Zeit (isothermische IOT) und Oxidations-Induktions-Temperatur (dynamische OIT)*

— *Teil 7: Bestimmung der Kristallisationskinetik*

Entsprechend der CEN-CENELEC-Geschäftsordnung sind die nationalen Normungsinstitute der folgenden Länder gehalten, diese Europäische Norm zu übernehmen: Belgien, Bulgarien, Dänemark, Deutschland, die ehemalige jugoslawische Republik Mazedonien, Estland, Finnland, Frankreich, Griechenland, Irland, Island, Italien, Kroatien, Lettland, Litauen, Luxemburg, Malta, Niederlande, Norwegen, Österreich, Polen, Portugal, Rumänien, Schweden, Schweiz, Slowakei, Slowenien, Spanien, Tschechische Republik, Türkei, Ungarn, Vereinigtes Königreich und Zypern.

Anerkennungsnotiz

Der Text von ISO 11357-4:2014 wurde vom CEN als EN ISO 11357-4:2014 ohne irgendeine Abänderung genehmigt.

1 Anwendungsbereich

Dieser Teil von ISO 11357 legt Verfahren zur Bestimmung der spezifischen Wärmekapazität von Kunststoffen mittels Dynamischer Differenz-Thermoanalyse (Dynamischer Differenzkalorimetrie) fest.

2 Normative Verweisungen

Die folgenden zitierten Dokumente, die in diesem Dokument teilweise oder als Ganzes zitiert werden, sind für die Anwendung dieses Dokuments erforderlich. Bei datierten Verweisungen gilt nur die in Bezug genommene Ausgabe. Bei undatierten Verweisungen gilt die letzte Ausgabe des in Bezug genommenen Dokuments (einschließlich aller Änderungen).

ISO 472, *Plastics — Vocabulary*

ISO 11357-1, *Plastics — Differential scanning calorimetry (DSC) — Part 1: General principles*

ISO 80000-1, *Quantities and units — Part 1: General*

3 Begriffe

Für die Anwendung dieses Dokuments gelten die Begriffe nach ISO 472 und ISO 11357-1 und die folgenden Begriffe.

3.1
Kalibriersubstanz
Substanz mit bekannter spezifischer Wärmekapazität

Anmerkung 1 zum Begriff: Als Kalibriersubstanz wird üblicherweise α-Aluminiumoxid (wie z. B. synthetischer Saphir) mit einem Reinheitsgrad von 99,9 % oder höher verwendet.

3.2
spezifische Wärmekapazität (bei konstantem Druck)
c_p
erforderliche Wärmemenge, um die Temperatur einer Substanz der Einheitsmasse bei konstantem Druck um 1 K zu erhöhen

Anmerkung 1 zum Begriff: Sie ist durch die folgende Gleichung gegeben:

$$c_p = m^{-1}C_p = m^{-1}(dQ/dT)_p \quad (1)$$

Dabei ist

m die Masse der Substanz;

C_p die Wärmekapazität in Kilojoule je Kilogramm je Kelvin ($kJ \cdot kg^{-1} \cdot K^{-1}$) oder in Joule je Gramm je Kelvin ($J \cdot g^{-1} \cdot K^{-1}$) angegeben, p kennzeichnet einen isobaren Vorgang;

dQ die erforderliche Wärmemenge, um die Temperatur der Substanz um dT zu erhöhen.

Anmerkung 2 zum Begriff: Diese Gleichung gilt in einem Temperaturbereich, in dem die Substanz keine Phasenumwandlung erster Ordnung zeigt.

$$(dQ/dT) = (dt/dT) \times (dQ/dt) = (\text{Heizrate})^{-1} \times (\text{Wärmestrom}) \quad (2)$$

Anmerkung 3 zum Begriff: Bei den Phasenumwandlungen liegt eine Diskontinuität in der Wärmekapazität vor. Ein Teil der Wärme wird zur Erzeugung eines Zustandes der Substanz mit höherer Energie verbraucht, so dass die Wärme nicht ausschließlich für das Erhöhen der Temperatur verbraucht wird. Daher kann die spezifische Wärmekapazität nur außerhalb der Phasenumwandlungsbereiche richtig bestimmt werden.

4 Kurzbeschreibung

4.1 Allgemeines

Jede Messung setzt sich aus drei Durchläufen bei der gleichen Abtastrate zusammen (siehe Bild 1):

a) eine Blindwertmessung (Leertiegel in Proben- und Referenzhaltern);

b) eine Kalibriermessung (Kalibriersubstanz im Tiegel im Probenhalter und Leertiegel im Referenzhalter);

c) eine Messung am Probekörper (Probekörper im Tiegel im Probenhalter und Leertiegel im Referenzhalter).

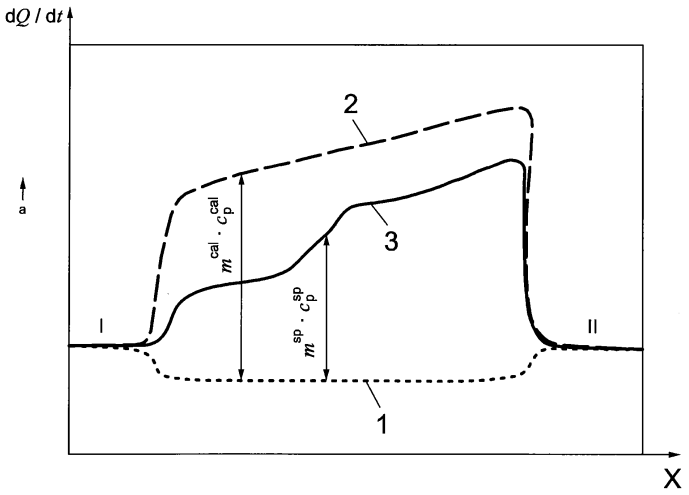

Legende

X Temperatur T oder Zeit t
1 Blindwertmessung
2 Kalibriermessung
3 Messung am Probekörper
I Isotherme Basislinie bei Anfangstemperatur T_s
II Isotherme Basislinie bei Endtemperatur T_f
a endotherme Richtung

Bild 1 — Schematische Darstellung typischer DSC-Kurven für die Messung spezifischer Wärmekapazität (Blindwertmessung, Kalibriermessung und Messung am Probekörper) nach Anpassung der Basislinie

4.2 Kontinuierliches Abtastverfahren

Basierend auf dem Prinzip der DSC (siehe ISO 11357-1) und der unter 3.2 angegebenen Definition der spezifischen Wärmekapazität können die folgenden Beziehungen aufgestellt werden:

$$m^{sp} \cdot c_p^{sp} \propto P_{Probekörpermessung} - P_{Blindwertmessung} \quad (3)$$

$$m^{cal} \cdot c_p^{cal} \propto P_{Kalibriermessung} - P_{Blindwertmessung} \quad (4)$$

Dabei ist

P der Wärmestrom (dQ/dt);

obere Indizes sp und cal bezeichnen den Probekörper und die Kalibriersubstanz (siehe Bild 1).

Wenn $P_{Probekörpermessung}$, $P_{Kalibriermessung}$ und $P_{Blindwertmessung}$ gemessen sind, kann c_p^{sp} nach Gleichung (6) berechnet werden, da die Werte von c_p^{cal}, m^{sp} und m^{cal} bekannt sind:

$$\frac{m^{sp} \cdot c_p^{sp}}{m^{cal} \cdot c_p^{cal}} = \frac{P_{Probekörpermessung} - P_{Blindwertmessung}}{P_{Kalibriermessung} - P_{Blindwertmessung}} \quad (5)$$

$$c_p^{sp} = c_p^{cal} \cdot \frac{m^{cal}\left(P_{Probekörpermessung} - P_{Blindwertmessung}\right)}{m^{sp}\left(P_{Kalibriermessung} - P_{Blindwertmessung}\right)} \quad (6)$$

4.3 Schrittweises Abtastverfahren

Im schrittweisen Abtastverfahren wird der gesamte abzutastende Temperaturbereich in kleine Intervalle unterteilt, und die unter 4.1 beschriebene gesamte Bestimmung, die sich aus drei Durchläufen zusammensetzt, wird für jedes Temperaturintervall durchgeführt. Nach Integration der Wärmestromkurve kann die im Intervall aufgenommene Gesamtwärme ΔQ erhalten werden. Eine Division von ΔQ durch das Temperaturintervall ΔT und die Masse des Probekörpers ergibt die spezifische Wärmekapazität [siehe Gleichung (1)]:

$$m^{sp} \cdot c_p^{sp} \propto \left(\frac{\Delta Q^{sp}}{\Delta T}\right)_p - \left(\frac{\Delta Q^{blank}}{\Delta T}\right)_p \quad (7)$$

$$m^{cal} \cdot c_p^{cal} \propto \left(\frac{\Delta Q^{cal}}{\Delta T}\right)_p - \left(\frac{\Delta Q^{blank}}{\Delta T}\right)_p \quad (8)$$

Werden die Temperaturintervalle ΔT konstant gehalten, ergibt sich beim Zusammenfassen der Gleichungen (7) und (8):

$$c_p^{sp} = c_p^{cal} \cdot \frac{m^{cal}}{m^{sp}} \cdot \frac{\Delta Q^{sp} - \Delta Q^{blank}}{\Delta Q^{cal} - \Delta Q^{blank}} \quad (9)$$

5 Geräte

5.1 DSC-Gerät. Siehe ISO 11357-1.

5.2 Tiegel. Siehe ISO 11357-1.

Die Tiegel für den Probekörper und den Referenz-Probekörper (Kalibriersubstanz) müssen die gleiche Form aufweisen und aus dem gleichen Werkstoff gefertigt sein, und deren Massen dürfen um nicht mehr als 0,1 mg voneinander abweichen.

ANMERKUNG Dieselbe Blindwertmessung und Kalibriermessung können für mehrere Messungen angewendet werden, wenn das Gerät ausreichend stabil ist und eine Korrektur hinsichtlich des Massenunterschieds zwischen dem Tiegel mit der Kalibriersubstanz und dem Leertiegel vorgenommen wurde. Eine geeignete Korrektur kann erzielt werden, indem der Term $c_{p,crucible}(T)\beta\Delta m$ zum Wärmestrom der Kalibriermessung addiert wird, wobei $c_{p,crucible}(T)$ die spezifische Wärmekapazität des Kalibriertiegels als Funktion der Temperatur, β die Heizrate und Δm der Massenunterschied zwischen dem Kalibriertiegel und dem Leertiegel sind. Das gleiche Verfahren kann ebenfalls für die Korrektur hinsichtlich der Massenunterschiede zwischen der Messung am Probekörper und der Blindwertmessung angewendet werden.

5.3 Analysenwaage. Siehe ISO 11357-1.

6 Probekörper

Siehe ISO 11357-1.

7 Prüfbedingungen und Konditionieren der Probekörper

Siehe ISO 11357-1.

8 Durchführung

8.1 Auswahl der Tiegel

Es sind drei Tiegel und deren Deckel vorzubereiten und die Tiegel sind zusammen mit deren Deckeln zu wägen. Die Gesamtmasse darf um nicht mehr als 0,1 mg (siehe 5.2) abweichen. In anderer Hinsicht, wie z. B. Werkstoff, Größe, Art des Tiegels (offen oder verschlossen), müssen die Tiegel identisch sein.

8.2 Einrichten des Geräts und Anpassen der isothermen Basislinien

8.2.1 Zwei Leertiegel mit Deckeln sind in den Proben- und Referenzhalter des DSC-Geräts einzusetzen.

8.2.2 Beim Anwenden eines kontinuierlichen Abtastprogramms:

a) Die Anfangs- und Endtemperatur (T_s und T_f) sind einzustellen. Die Anfangstemperatur T_s sollte um mindestens 30 K tiefer liegen als diejenige, bei der Daten zuerst benötigt werden.

ANMERKUNG 1 Wenn genauere Ergebnisse über einen weiten Temperaturbereich gefordert werden, kann der Gesamtbereich in zwei (oder mehr) kleinere Bereiche unterteilt werden, jeder 50 K bis 100 K breit. Die Anfangstemperatur T_s des zweiten Bereiches sollte um 30 K tiefer liegen als die Endtemperatur T_f des ersten Temperaturbereiches, um eine ausreichende Überlappung sicherzustellen.

b) Die Abtastrate ist einzustellen.

c) Das Zeitintervall zwischen den isothermen Phasen I und II (siehe Bild 1) ist einzustellen und es ist abzuwarten, bis sich die jeweiligen isothermen Basislinien stabilisiert haben. Dieses Intervall beträgt üblicherweise 2 min bis 10 min.

ANMERKUNG 2 Einige Kalorimeter, z. B. vom Calvet-Typ, können bis zu 30 min in Anspruch nehmen, bis sich die Basislinie stabilisiert hat.

8.2.3 Beim Anwenden eines schrittweisen Abtastprogramms:

Wenn die spezifischen Wärmekapazitäten der Proben keine beträchtliche Abhängigkeit von der Temperatur zeigen, kann das schrittweise Abtastverfahren angewendet werden, bei dem die Integration des Wärmestroms über kleine Temperaturintervalle einen Satz einzelner Werte der spezifischen Wärmekapazität für die betrachteten Temperaturintervalle liefert. Es ist auf Folgendes zu achten:

a) Um eine stabile Basislinie zu erhalten, muss das Zeitintervall zwischen den isothermen Phasen ausreichend groß sein.

b) Dieses Verfahren darf nicht in einem Temperaturbereich angewendet werden, in dem Phasenumwandlungen erster Ordnung auftreten.

Die schrittweise Abtastung wird wie folgt durchgeführt:

— Die Anfangs- und Endtemperatur (T_s und T_f) sind einzustellen.

— Der Temperaturzuwachs ist vorzugsweise auf 5 K bis 10 K einzustellen.

— Die Temperaturabtastrate ist auf 5 K·min^{-1} oder 10 K·min^{-1} einzustellen.

— Das Zeitintervall zwischen den isothermen Phasen ist einzustellen; dieses beträgt üblicherweise 2 min bis 10 min.

8.2.4 Die Empfindlichkeit des Wärmestroms ist einzustellen, um eine Ordinatenspannweite von mindestens 80 % der gesamten Skala zu erhalten (siehe Bild 1).

8.2.5 Das Gerät ist so einzustellen, dass die isothermen Basislinien vor und nach der Heizphase sich auf dem gleichen Ordinatenniveau befinden.

Werden mikrocomputerbasierte Systeme verwendet, können die isothermen Basislinien nach dem Erhalten der Daten an das gleiche Ordinatenniveau angepasst werden. Es wird jedoch dringend empfohlen, das Anpassen der Basislinie vor der Durchführung jeglicher Messungen vorzunehmen, um die Präzision der Ergebnisse zu erhöhen. Wird ein üblicher Schreiber verwendet, ist eine korrekte Einstellung des Geräts entscheidend, um die Unterschiede im Niveau der isothermen Basislinien zu minimieren.

Es ist zu überprüfen, ob das Anpassen der Basislinien der jeweiligen DSC-Kurven das gleiche Ordinatenniveau ergibt. Ist die Basislinienreproduzierbarkeit schlecht, so ist das Gerät neu einzustellen und die Bestimmung zu wiederholen.

ANMERKUNG Weitere Gründe für eine schlechte Basislinienreproduzierbarkeit können eine Kontamination des Probentiegels, die Position des Deckels, die Stabilität der Spülgasdurchflussrate, eine Probenzersetzung, eine Probenverdampfung, eine chemische Reaktion zwischen dem Tiegel und der Probe usw. sein.

8.2.6 Das Temperaturprogramm, das wie in 8.2.2 oder 8.2.3 beschrieben eingestellt ist, ist durchzuführen. In Bild 2 ist eine typische, im kontinuierlichen Abtastmodus erhaltene DSC-Kurve dargestellt und in Bild 3 eine im schrittweisen Abtastmodus erhaltene DSC-Kurve.

8.3 Messung der spezifischen Wärmekapazität der Kalibriersubstanz

Mithilfe einer Analysenwaage ist eine Kalibriersubstanz, wie z. B. α-Aluminiumoxid (synthetischer Saphir) mit einem Reinheitsgrad von 99,9 % oder höher in einen der nach 8.1 vorbereiteten Tiegel einzuwägen. Der die Kalibriersubstanz enthaltende Tiegel mit dem Deckel ist in den Probenhalter einzusetzen und eine DSC-Messung durchzuführen.

ANMERKUNG 1 Eine Korrektur hinsichtlich geringer Massenunterschiede der Tiegel, die für die Messung am Probekörper, Kalibriermessung und Blindwertmessung verwendet werden, kann, wie in der Anmerkung zu 5.2 beschrieben, vorgenommen werden.

ANMERKUNG 2 Um systematische Fehler zu verringern, sollte die Wärmekapazität der Kalibriersubstanz der des zu analysierenden Probekörpers möglichst weit entsprechen.

Für die Blindwertmessung sind andere Leertiegel, vorbereitet nach 8.1, zu verwenden. Es ist (sind) die gleiche(n) Messung(en) durchzuführen, wie unter 8.2 beschrieben. Die Nennwerte der spezifischen Wärmekapazität von α-Aluminiumoxid bei verschiedenen Temperaturen sind in Tabelle A.1 angegeben.

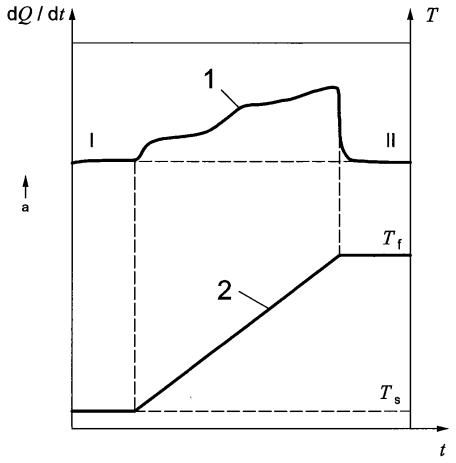

Legende

1 DSC-Kurve
2 Temperaturkurve
I Isotherme Basislinie bei Anfangstemperatur T_s
II Isotherme Basislinie bei Endtemperatur T_f
a endotherme Richtung

Bild 2 — Schematische Darstellung einer im kontinuierlichen Abtastverfahren aufgenommenen DSC-Kurve

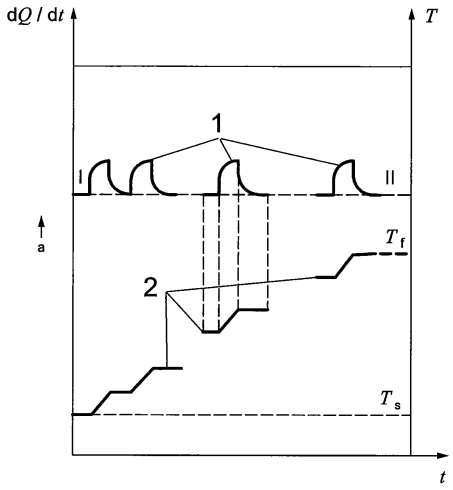

Legende

1 DSC-Kurve
2 Temperaturkurve
I Isotherme Basislinie bei Anfangstemperatur T_s
II Isotherme Basislinie bei Endtemperatur T_f
a endotherme Richtung

Bild 3 — Schematische Darstellung einer im schrittweisen Abtastverfahren aufgenommenen DSC-Kurve

8.4 Messung am Probekörper

Der Probekörper ist in den Probentiegel einzuwägen. Der den Probekörper enthaltende Tiegel mit dem Deckel ist in den Probenhalter einzusetzen, und eine DSC-Messung ist wie für die Kalibriersubstanz durchzuführen. Es wird eine große Probenmasse empfohlen.

Dieselbe Blindwertmessung, die für die Kalibriermessung nach 8.3 angewendet wurde, kann ebenfalls für die Messung am Probekörper angewendet werden.

9 Bestimmung spezifischer Wärmekapazitäten

9.1 Berechnung spezifischer Wärmekapazitäten

Es ist c_p^{sp} nach Gleichung (6) bei der kontinuierlichen Aufheizung oder nach Gleichung (9) beim schrittweisen Verfahren in $J \cdot g^{-1} \cdot K^{-1}$ zu berechnen.

9.2 Numerische Rundung der Ergebnisse

Die so erhaltenen Werte der spezifischen Wärmekapazität sind unter Anwendung des in ISO 80000-1 festgelegten Verfahrens auf die zweite Dezimalstelle zu runden.

10 Präzision und systematische Messabweichung

Die Präzision und systematische Messabweichung der beschriebenen Verfahren ist nicht bekannt, weil kein Ringversuch durchgeführt wurde. Angaben zur Präzision werden aufgenommen, sobald Daten in ausreichender Menge vorliegen.

11 Prüfbericht

Der Prüfbericht muss folgende Angaben enthalten:

a) eine Verweisung auf diesen Teil von ISO 11357;

b) Prüfdatum;

c) alle zur vollständigen Identifizierung der geprüften Probe erforderlichen Einzelheiten, einschließlich thermische Vorgeschichte;

d) Hersteller, Modell und Typ (leistungskompensiertes Kalorimeter oder Wärmestrom-Differenz-Kalorimeter) des verwendeten DSC-Geräts;

e) Form, Maße und Werkstoffe des Tiegels und Deckels;

f) Prüfatmosphäre und Durchflussrate des Spülgases;

g) Kalibriersubstanz, einschließlich Informationen zur erteilenden Stelle, Art der Substanz, die verwendete Masse und andere für die Kalibrierung relevante Merkmale;

h) Form, Maße und Masse des Probekörpers;

i) Einzelheiten zur Probenahme und Konditionierung des Probekörpers;

j) Parameter des Temperaturprogramms, d. h. Anfangstemperatur, Heizrate, Endtemperatur, Zeitintervall zwischen den isothermen Phasen und beim Verfahren mit schrittweise erfolgender Aufheizung des Temperaturzuwachs sowie die Abkühlrate beim Konditionieren, falls durchgeführt;

k) Prüfergebnisse, einschließlich spezifische Wärmekapazitäten und entsprechende Temperaturen;

l) gegebenenfalls weitere erforderliche Angaben.

Anhang A
(informativ)

Annäherungsausdruck für die spezifische Wärmekapazität des reinen α-Aluminiumoxids [3] bis [5]

Die Werte der spezifischen Wärmekapazität in Tabelle A.1 sind durch die folgenden Gleichungen angenähert:

$$c_p = A_0 + A_1 x + A_3 x^{2\ N1)} + A_3 x^3 + A_4 x^4 + A_5 x^5 + A_6 x^6 + A_7 x^7 + A_8 x^8 + A_9 x^9 + A_{10} x^{10} \quad \text{(A.1)}$$

$$x = (T\,\text{K} - 650\,\text{K})/550\,\text{K} \quad \text{(A.2)}$$

$$= (\theta\,°\text{C} - 376{,}85\,°\text{C})/550\,°\text{C} \quad \text{(A.3)}^{N2)}$$

$$\theta\,°\text{C} = T\,\text{K} - 273{,}15\,\text{K} \quad \text{(A.4)}^{N3)}$$

Dabei ist

$100\,\text{K} \leq T \leq 1\,200\,\text{K}$

und

$A_0 = 1{,}127\,05$

$A_1 = 0{,}232\,60$

$A_2 = -0{,}217\,04$

$A_3 = 0{,}264\,10$

$A_4 = -0{,}237\,78$

$A_5 = -0{,}100\,23$

$A_6 = 0{,}153\,93$

$A_7 = 0{,}545\,79$

$A_8 = -0{,}478\,24$

$A_9 = -0{,}376\,23$

$A_{10} = 0{,}344\,07$

und

c_p und A_i $(i = 1, 2, ...)$ sind in $\text{J}\cdot\text{g}^{-1}\cdot\text{K}^{-1}$;

T ist in K;

θ ist in °C.

Die Koeffizienten in den Gleichungen (A.2) und (A.2a) dienen der Normierung der Temperaturvariablen T und θ.

Die Standardabweichung von den Werten in Tabelle A.1 beträgt 0,000 13 $\text{J}\cdot\text{g}^{-1}\cdot\text{K}^{-1}$.

Die maximale Abweichung beträgt 0,071 % bei 140 K.

N1) Dieser Index in der ISO 11357-4:2014 ist falsch. Die richtige Angabe lautet „A_2x^2".

N2) Dieser Index in der ISO 11357-4:2014 ist falsch. Die richtige Angabe lautet „(A.2a)".

N3) Dieser Index in der ISO 11357-4:2014 ist falsch. Die richtige Angabe lautet „(A.3)".

Die Standardabweichung bei Temperaturen über 300 K beträgt weniger als 0,02 %.

Tabelle A.1 — Spezifische Wärmekapazität des reinen α-Aluminiumoxids im Temperaturbereich von 120 K bis 780 K [3] bis [5]

Temperatur		Spezifische Wärmekapazität	Temperatur		Spezifische Wärmekapazität
K	°C	$J \cdot g^{-1} \cdot K^{-1}$	K	°C	$J \cdot g^{-1} \cdot K^{-1}$
120,00	−153,15	0,196 9	440,00	166,85	0,987 5
130,00	−143,15	0,235 0	450,00	176,85	0,997 5
140,00	−133,15	0,274 0	460,00	186,85	1,007 0
150,00	−123,15	0,313 3	470,00	196,85	1,016 0
160,00	−113,15	0,352 5	480,00	206,85	1,024 7
170,00	−103,15	0,391 3	490,00	216,85	1,033 0
180,00	−93,15	0,429 1	500,00	226,85	1,040 8
190,00	−83,15	0,465 9	510,00	236,85	1,048 4
200,00	−73,15	0,501 4	520,00	246,85	1,055 6
210,00	−63,15	0,535 5	530,00	256,85	1,062 6
220,00	−53,15	0,568 2	540,00	266,85	1,069 2
230,00	−43,15	0,599 4	550,00	276,85	1,075 6
240,00	−33,15	0,629 2	560,00	286,85	1,081 6
250,00	−23,15	0,657 6	570,00	296,85	1,087 5
260,00	−13,15	0,684 5	580,00	306,85	1,093 1
270,00	−3,15	0,710 1	590,00	316,85	1,098 6
280,00	6,85	0,734 2	600,00	326,85	1,103 8
290,00	16,85	0,757 1	610,00	336,85	1,108 8
300,00	26,85	0,778 8	620,00	346,85	1,113 6
310,00	36,85	0,799 4	630,00	356,85	1,118 2
320,00	46,85	0,818 6	640,00	366,85	1,122 7
330,00	56,85	0,837 2	650,00	376,85	1,127 0
340,00	66,85	0,854 8	660,00	386,85	1,131 3
350,00	76,85	0,871 3	670,00	396,85	1,135 3
360,00	86,85	0,887 1	680,00	406,85	1,139 2
370,00	96,85	0,902 0	690,00	416,85	1,143 0
380,00	106,85	0,916 1	700,00	426,85	1,146 7
390,00	116,85	0,929 5	720,00	446,85	1,153 7
400,00	126,85	0,942 3	740,00	466,85	1,160 4
410,00	136,85	0,954 4	760,00	486,85	1,166 7
420,00	146,85	0,966 0	780,00	506,85	1,172 6
430,00	156,85	0,977 0			

F Sapphire simulation results

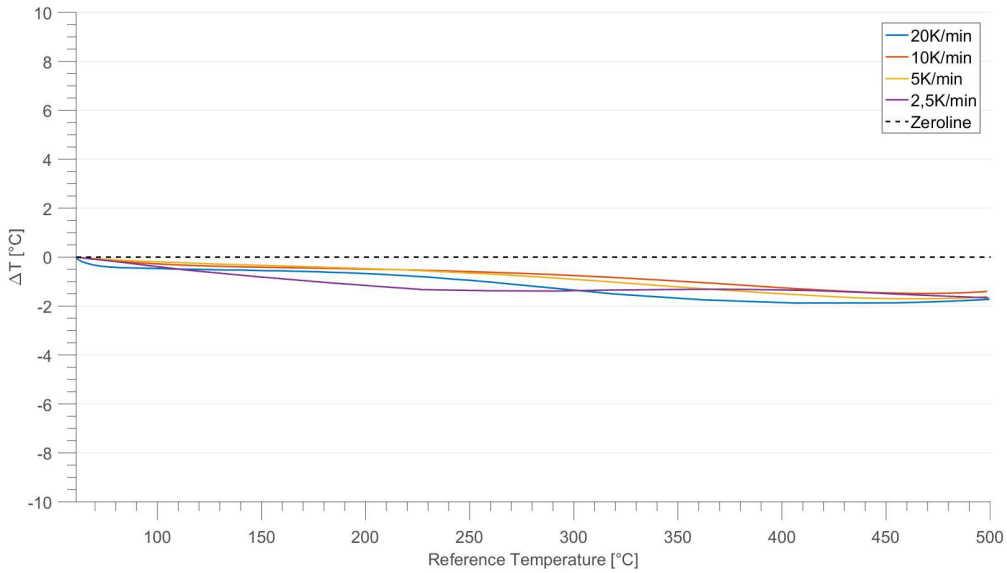

Figure 3: Difference between the simulated and the measured sample temperature for the sample of $m = 42,15mg$

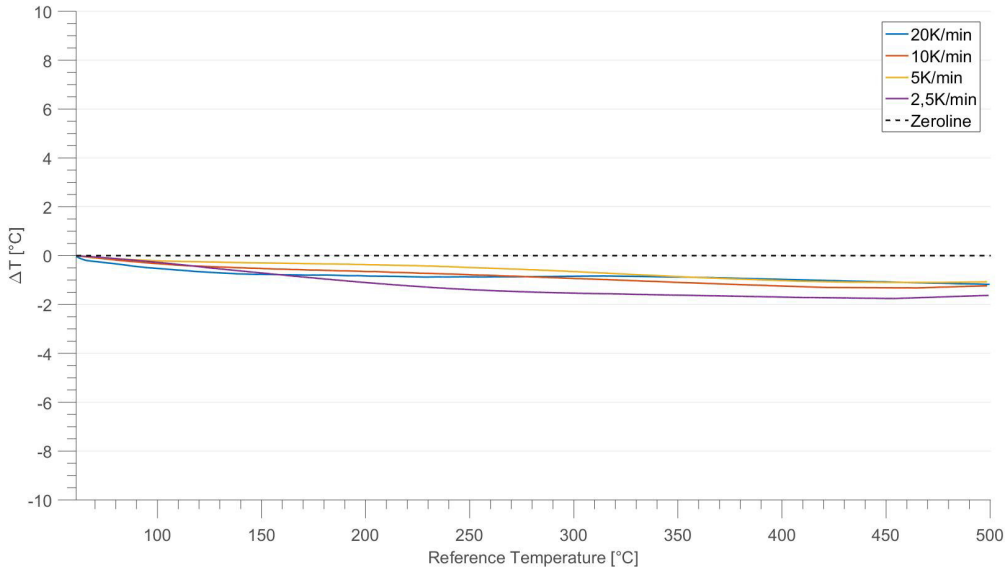

Figure 4: Difference between the simulated and the measured sample temperature for the sample of $m = 63,66mg$

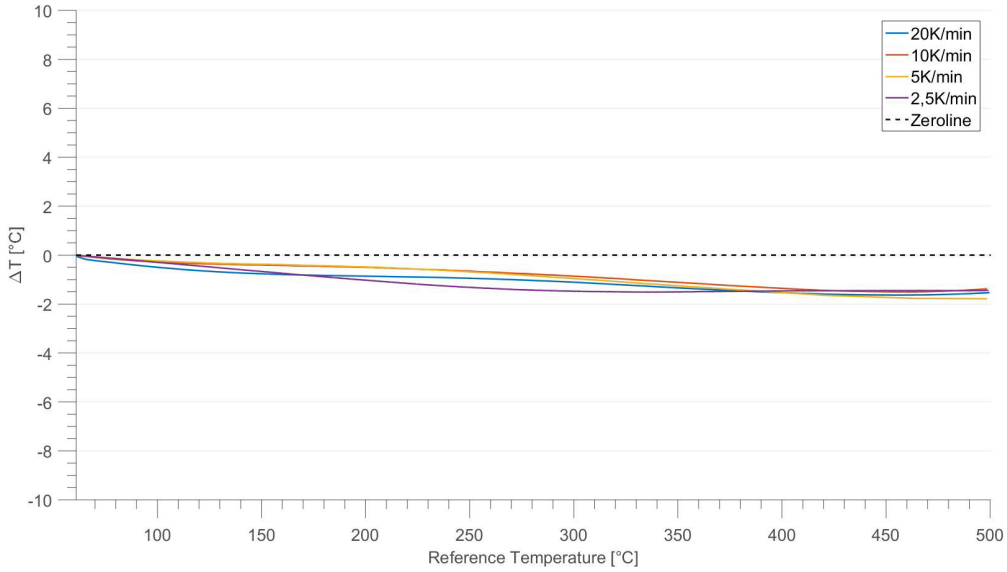

Figure 5: Difference between the simulated and the measured sample temperature for the sample of $m = 84,73mg$

G Polymer simulation results

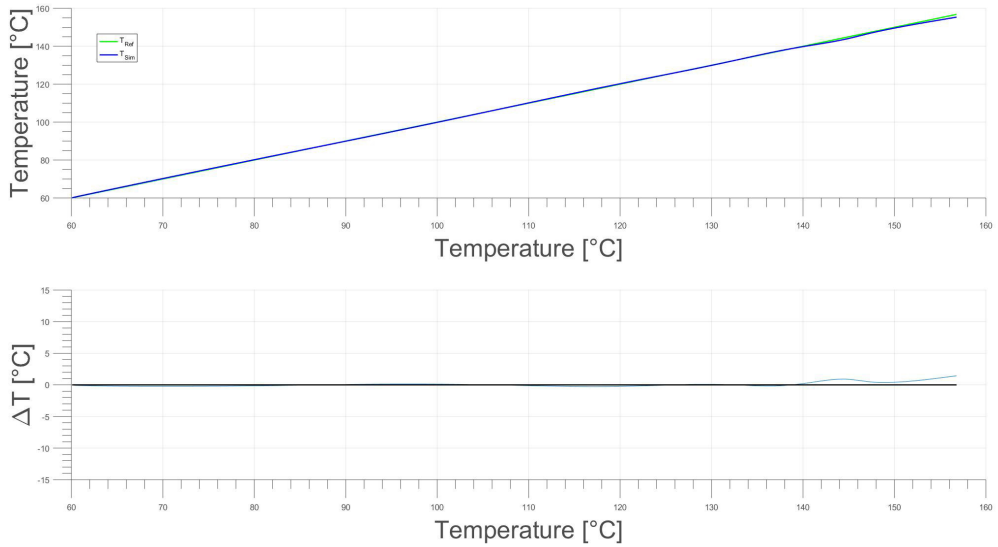

Figure 6: m=10,47, β=20K/min

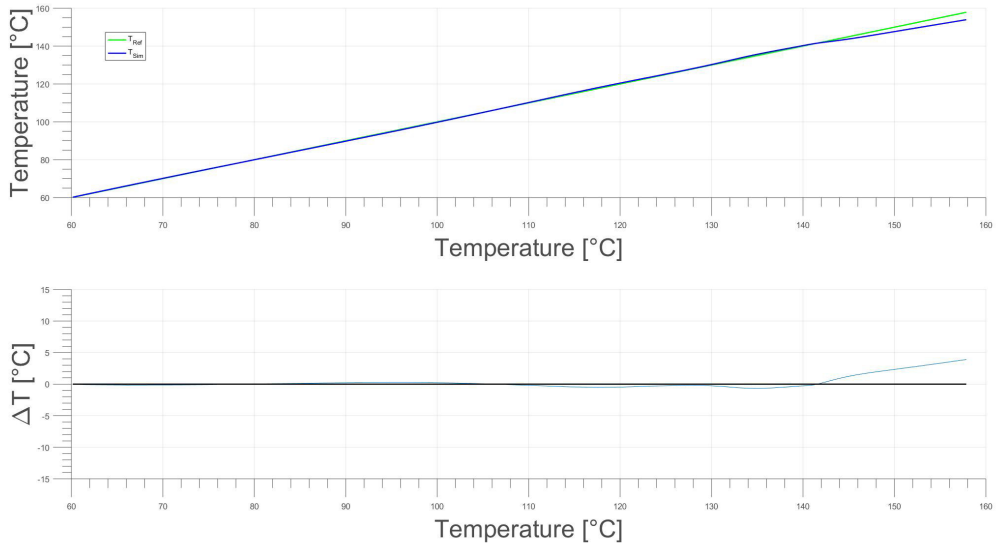

Figure 7: m=10,47, β=10K/min

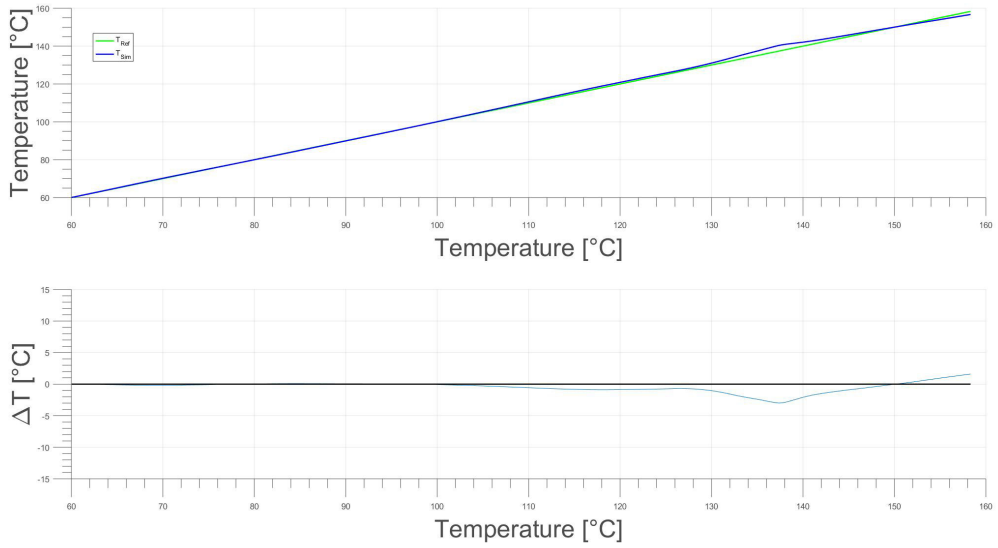

Figure 8: m=10,47, β=5K/min

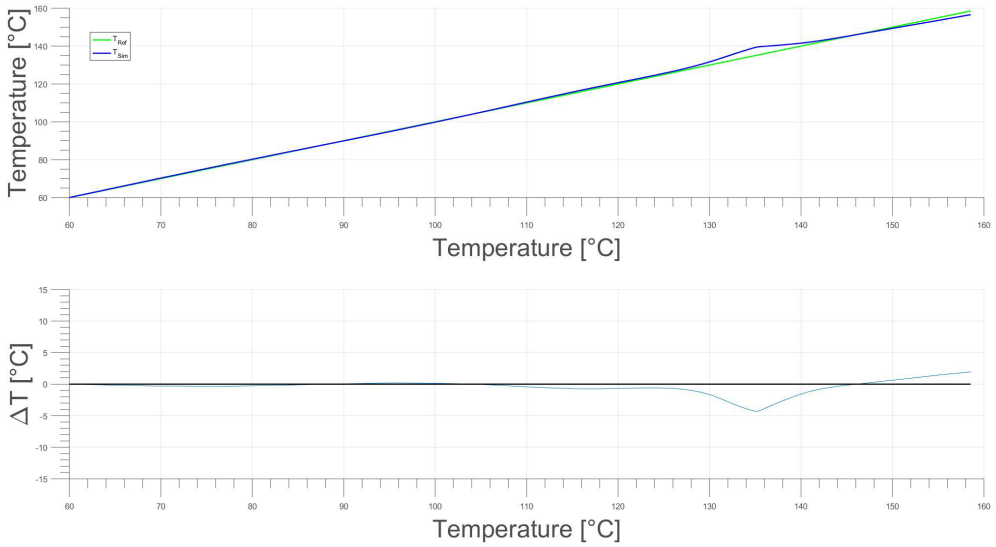

Figure 9: m=10,47, β=2,5K/min

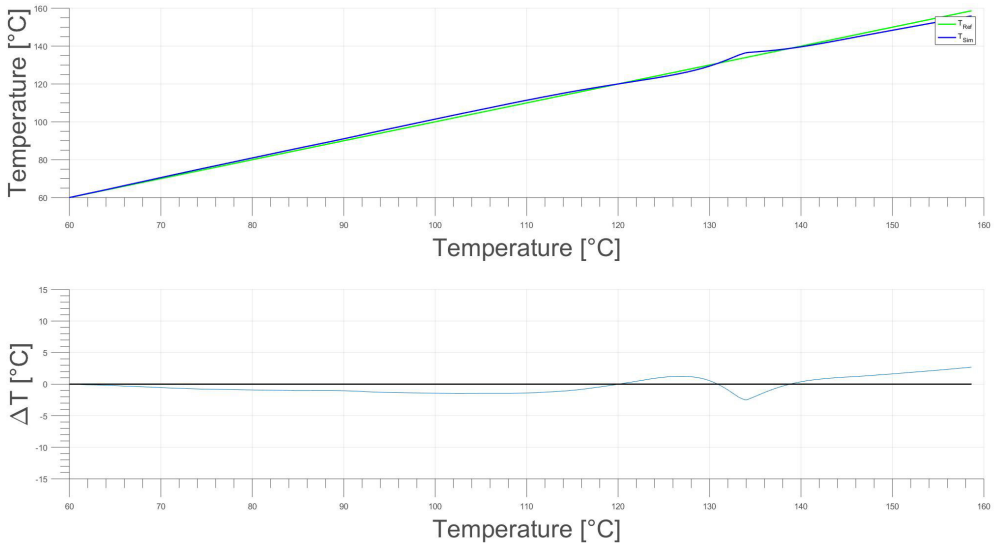

Figure 10: m=10,47, β=1,25K/min